Estimates of Time and Space Scales at 300 Meters in the Midlatitude North Pacific from the TRANSPAC XBT Program

LYNNE D. TALLEY AND WARREN B. WHITE

Scripps Institution of Oceanography, University of California, San Diego, La Jolla, CA 92093

(Manuscript received 30 December 1986, in final form 5 June 1987)

ABSTRACT

Estimates of length and time scales of temperature variability at 300 meters in the midlatitude North Pacific are made. Data are XBT traces collected from 1976 to 1984 in the TRANSPAC Volunteer Observing Ship program. Temperatures at 300 meters are grouped in two-month bins and gridded using the Surface II mapping program.

Temperature variance about the time mean is largest in the Kuroshio Extension and nearly constant in the eastern North Pacific. A cooling trend occurred in the eastern North Pacific over the eight years of the dataset. In the western Pacific, the annual cycle is most intense 1°–2° north of the Kuroshio Extension, with an indication of meridional propagation away from the region of most intense variability. Propagation of annual waves in the eastern Pacific was predominantly northwestward.

Wavenumber and frequency spectra are computed from normalized temperatures with the mean and bimonthly average removed in order to eliminate the dominant annual cycle. Based on the overall temperature variance, the North Pacific was divided into western and eastern regions. Zonal wavenumber and frequency spectra and two-dimensional ω/k spectra were computed for a number of latitudes in the eastern and western regions. Two-dimensional k/l spectra were also computed for the western and eastern regions. The spectra indicate westward propagation throughout the midlatitude North Pacific with additional eastward propagation in the Kuroshio Extension region, shorter length and time scales in the Kuroshio Extension compared with other regions, and slight dominance of southwestward propagation in both the eastern and western North Pacific.

Tests to determine the effective spatial resolution of the dataset indicate that local average-station spacing is a good measure of local Nyquist wavelength. However, because of the nearly random sampling in a spatially limited region, an unresolved wave is aliased more or less in a band stretching towards low wavenumber rather than folded in coherent, predictable locations in the spectrum. With the choice of a two-month time bin, spectra are about equally aliased in space and time, with Nyquist wavelength and period close to the beginning of energy rolloff reported in other surveys, which have better spatial resolution but less degrees of freedom.

1. Introduction

Studies of space–time scales in the North Pacific are numerous and have been based on a variety of data sources, including the TRANSPAC XBT dataset used in the present study, moored arrays, and satellite altimetry. The last has the most potential for describing surface structure, but XBT programs will continue to be an appropriate data source for subsurface structure. The TRANSPAC program is the only extant dataset from which a description of the space–time structure of the uppermost layer of the midlatitude North Pacific over a long period can be attempted. Because of the apparent richness of the dataset, we have felt it only fair to make the attempt; however, the density of observations in time and space means that aliasing is a fundamental problem. Resolution is considered to some extent in this paper, although an exhaustive analysis including determination of the best descriptor of subsurface variability from XBT data has not been done.

What has been learned from previous studies of space and time scales of temperature and velocity in the North Pacific? We know that the zonal wavenumber spectrum is red, with most energy at wavelengths longer than 250 km. Meridional scales are more difficult to determine unambiguously because of inhomogeneity in energy levels and physical processes in the meridional direction. The frequency spectrum is essentially red, with most energy at periods longer than 15 days. We have not had a clear picture of how both space and time scales change across the ocean.

A number of papers have related variability in this XBT dataset to Rossby wave structure. One observation is a clear decrease in spectral energy with increasing distance from the Kuroshio Extension and hence a strong division between a western and an eastern North Pacific regime (Bernstein and White, 1977). A second robust feature of space–time datasets in the subtropical Pacific is westward propagation of temperature variability (e.g., White, 1982), an intrinsic property of free Rossby wave activity. Only in the west has evidence

for eastward propagation been found (Mizuno and White, 1983), presumably due to strong advection by the Kuroshio Extension. It has therefore been natural to attempt to relate the variability found oceanwide to baroclinic Rossby wave activity. There have been discussions of annual Rossby waves, long baroclinic Rossby waves, sources of Rossby waves, the direction of Rossby-wave propagation, and consistency fits of Rossby waves to data. Waves in the western midlatitude North Pacific in the vicinity of the Kuroshio Extension have been treated by Bernstein and White (1982), Mizuno and White (1983), and White and He (1986). Wave activity in the eastern midlatitude North Pacific has been discussed by Kang and Magaard (1980), White and Saur, (1981), White (1982), White and Saur (1983), Mysak (1983), Price and Magaard (1983), and White (1985). All of the mentioned studies were conducted on portions of the TRANSPAC XBT dataset (White and Bernstein, 1979) using a variety of statistical procedures and models, both to demonstrate the presence of linear Rossby waves and to establish their sources. Demonstration of the existence of a Rossby-wave dispersion relation has never been as clean as desired, presumably because of the presence of nonlinearities, instabilities, and mean flow, all of which would alter the dispersion relation, and because of anisotropy of the background mean flow.

None of the previous studies has used the complete TRANSPAC XBT dataset, extending from North America to Japan, and a uniform analysis technique. In the present study the full 8 years of XBT data collected from 1976–84 (Fig. 1) are used to quantify dominant length and time scales and phase propagation direction across the North Pacific between 34° and 42°N. This impressively long time series spanning the northern part of the subtropical gyre certainly provides a well-determined mean and variance. However, the TRANSPAC sampling is somewhat inadequate in both time and space for determining the full space–time spectrum of mesoscale and large-scale structures. Some effort is expended here in understanding the limitations of the sampling scheme. In this respect, we are following Koblinsky et al. (1984), who examined the extent to which this dataset could be used to produce synoptic maps of a portion of the Kuroshio Extension.

Several previous studies of long baroclinic waves in the eastern midlatitude North Pacific employed a filter to extract the so-called "mesoscale" variability from the TRANSPAC data (Kang and Magaard, 1980; White, 1982, 1985). This high-pass filter combined with the low-pass gridding procedure creates a rather narrow-band filter. In the present study the high-pass filter is replaced with division by the standard deviation of temperature about the time mean, which suppresses

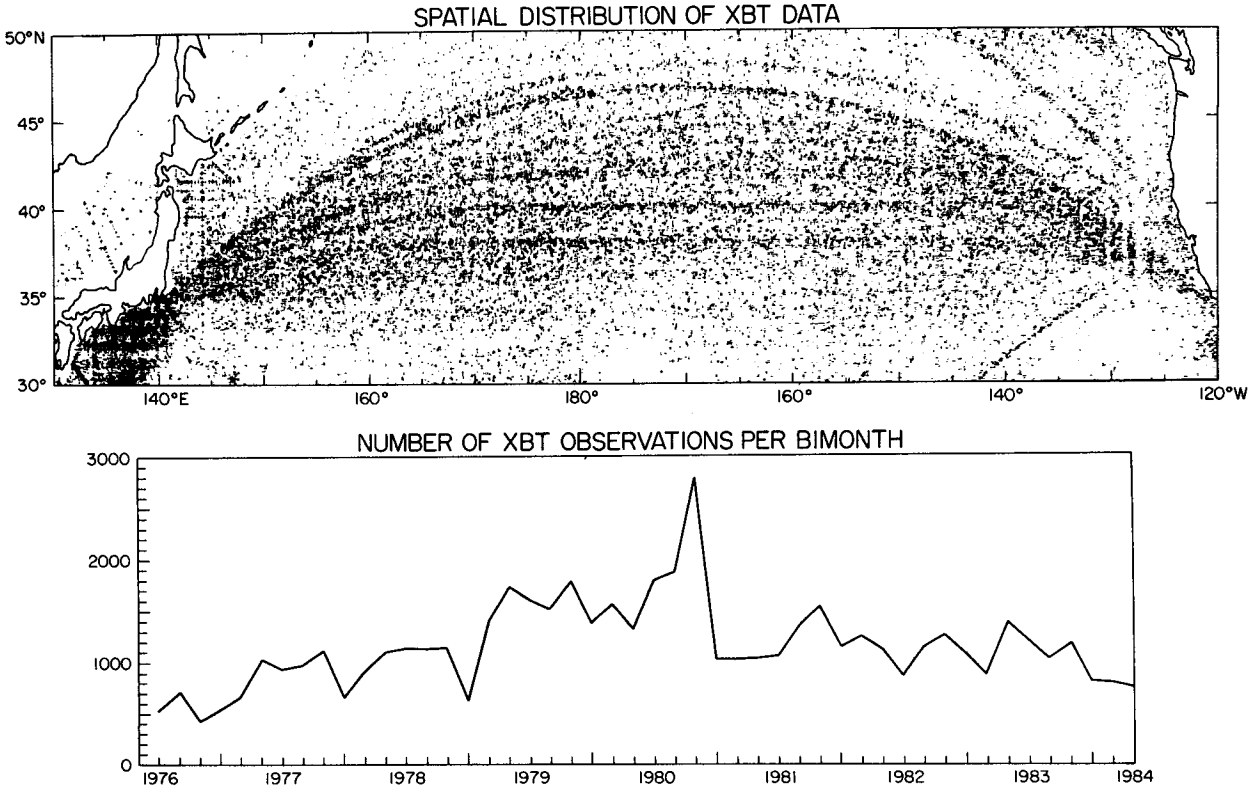

FIG. 1. (a) All XBT observations in the TRANSPAC dataset from June 1976 to May 1984. (b) Number of XBT observations in each two-month period (June–July, August–September, etc.) for the period 1976–84. Large tic-marks correspond to December–January.

spatial inhomogeneity in energy levels. Analysis is also improved by restriction to regions where average station spacing is less than 2° latitude/longitude over a two-month period.

The basic dataset and method are described in section 2. In section 3 and in an appendix, we explore the extent to which length and time scales of variability in the midlatitude North Pacific can be resolved with the present dataset and with the spectral methods and filters we have chosen. In section 4, we examine the eight-year mean, rms differences about the mean, the annual cycle itself, and anomalies (mean and annual cycle removed) of temperature at 300 m. Since this dataset has been analyzed in a number of other recent papers. we concentrate only on those aspects which are new or enhanced by the additional 4 years of observations, and those which are important for spectral analysis. Spectral results are presented in section 5. Because the sampling density precludes unaliased spectra of mesoscale phenomena, we have been cautious in interpreting results.

2. Method

Data used were TRANSPAC XBT observations from June 1976 to May 1984. All data points are shown in Fig. 1 along with the total number of points in each two-month interval. Data coverage is irregular and has a strong seasonal bias. Only those portions of the region which could be "adequately" sampled were included in this analysis; since the TRANSPAC XBT program was designed to sample large-scale features in space and time (White and Bernstein, 1979), it was barely adequate for mesoscale studies, allowing only wavelength scales of $L \geq 400$ km to be resolved each bimonth. Sampling was increased during a special six-month observing period in fall/winter of 1980/81, allowing shorter wavelengths (i.e., $L \geq 200$ km) to be resolved each month.

Continuous analog XBT traces were digitized every 5 meters and subsampled every 20 meters. A time bin of two months was chosen, with all observations within the period weighted equally. The Surface II mapping program (henceforth referred to as S2) was then used to interpolate the irregularly spaced temperature observations onto a regular ½° latitude/longitude spatial grid from each two-month group of observations (Sampson, 1973). Koblinsky et al. (1984) found that the interpolation procedure used by S2 performs as well as optimum interpolation for this dataset. In our application of the S2 interpolation procedure, the eight observations closest to the grid point are fit; the closest must be no more than 3° from the grid point and the farthest no more than 6° away. Therefore, the effective averaging radius about the grid point depends on local data density. If fewer than eight observations are found within a 6° radius of the grid point, then no interpolated value is produced. S2 uses a plane fit with weighting proportional to the inverse of distance from the grid point.

Forty-eight bimonthly grids of temperatures at 300 m were produced using S2 for observations from June 1976 to May 1984. The long-term mean and annual cycle in temperature were removed from the individual bimonthly gridded values by averaging all groups of bimonths together and subtracting these from the individual, bimonthly gridded values. This procedure also removes four- and six-month priods. The resulting 48 grids of anomalous temperature form our basic dataset.

3. Data resolution

In this section we consider when and where in the TRANSPAC data there is adequate resolution for description of the space–time structure of the temperature field, as well as problems of inhomogeneity and intermittency. Limitations arise from both the TRANSPAC data resolution and the gridding procedure. We first list various issues arising from the gridding method, and then test the sampling density and gridding and spectral methods by assigning a set of plane waves and, separately, random numbers to XBT observations. The random number test produces a response function for the method. Details of the tests are in an appendix; only the results are described here.

It has been shown that temperature at 300 m is a good descriptor of the mean and anomalous temperature of the upper portion of the main thermocline in the midlatitude North Pacific. A zonal section of XBT temperature in the upper 500 m along 38°N from 160°E to 140°W, taken by Bernstein and White (1977) with 80 km station spacing, finds the 300-m temperature to be an adequate descriptor of fluctuations in the main thermocline along the entire section. Meridional temperature sections displayed in the same study, extending from 30° to 40°N over that longitude range, summarized from Roden (1970, 1972), also demonstrated that 300 m lies within the main thermocline. On each section, both large-scale and mesoscale fluctuations tended to be vertically coherent throughout the upper portion of the main thermocline, from 200 to 500 m. On this basis, it is assumed that variability is dominated by low vertical modes, which has been demonstrated quantitatively by Emery and Magaard (1976) and Kang and Magaard (1980). Since the magnitude of the anomalies is enhanced where the main thermocline intersects 300 m and underestimated where it lies above and below 300 m, anomalies are normalized by the rms differences about the time mean at each grid point. Other descriptors of the anomalous thermal field, such as surface dynamic height, vertical empirical orthogonal functions, or available potential energy may offer a different perspective.

It is assumed that the mean and variance of temperature at each point are well determined by the eight years of data. This is a reasonable assumption over

most of the midlatitude North Pacific, but is not correct in the immediate vicinity of the Kuroshio Extension where the temperature distribution is bimodal, reflecting the large temperature change across the Kuroshio (Koblinsky et al., 1984). Mean temperatures at a point would be better estimated by separating groups of observations which are north and south of the Kuroshio Extension; rms differences would then be produced about the respective means in each group. Since we have not done this, the anomaly field in the Kuroshio region may be dominated by Kuroshio meandering (Koblinsky et al., 1984).

Data density in the TRANSPAC program is uneven (Fig. 1b) and has a pronounced seasonal bias. A given bimonth is usually sampled most densely in an arced band across the Pacific, with ships following the great circle route from Japan to North America. Choice of a time bin clearly dictates the spatial resolution. An attempt was made to balance the spatial and temporal sampling; a time bin of two months was chosen within which all XBT drops were weighted equally and considered to be synoptic. The bimonthly bin adequately resolves the evolution of large-scale temperature variability which has been shown to have a decorrelation time scale of 10 months and a space scale of 5°–15° latitude and 20°–30° longitude (White and Bernstein, 1979). It does not adequately resolve the mesoscale variability, which has a decorrelation time scale of one to two months and space scale of 150 to 200 km in the Kuroshio Extension (Bernstein and White, 1981; Koblinsky et al., 1984).

Spatial resolution is better than 2° over reasonably large portions of the North Pacific in most bimonths. Spatial resolution can be measured as a by-product of the S2 gridding procedure which uses the eight observations closest to a grid point out to a 6° radius. Therefore the size of the region over which S2 averages is determined by the local density of observations, so S2 is a low-pass filter with a variable averaging radius. For sufficiently large data density, the low-pass filter effect is reduced. The average distance to the eight points, $\bar{r}_8$, is an output of S2 and is related directly to the average separation between neighboring observations; this is approximately $\bar{r}_8/1.2$ if observations are uniformly distributed. The average separation between neighboring points therefore determines the length scales passed by the spectral method. Shorter scales are passed in regions where sampling density is higher. The Nyquist wavelength associated with an $\bar{r}_8$ of 2° is about 3.3°: if only regions with $\bar{r}_8$ less than 2° are used, all wavelengths longer than 3.3° are resolved while resolution of shorter wavelengths depends on the local $\bar{r}_8$. Because previous studies show that there is significant energy at wavelengths of 250–350 km throughout the North Pacific, the spatial spectra are aliased to some extent.

The spatial resolution of the dataset, using bimonthly time bins, is illustrated in Fig. 2 with maps of XBT

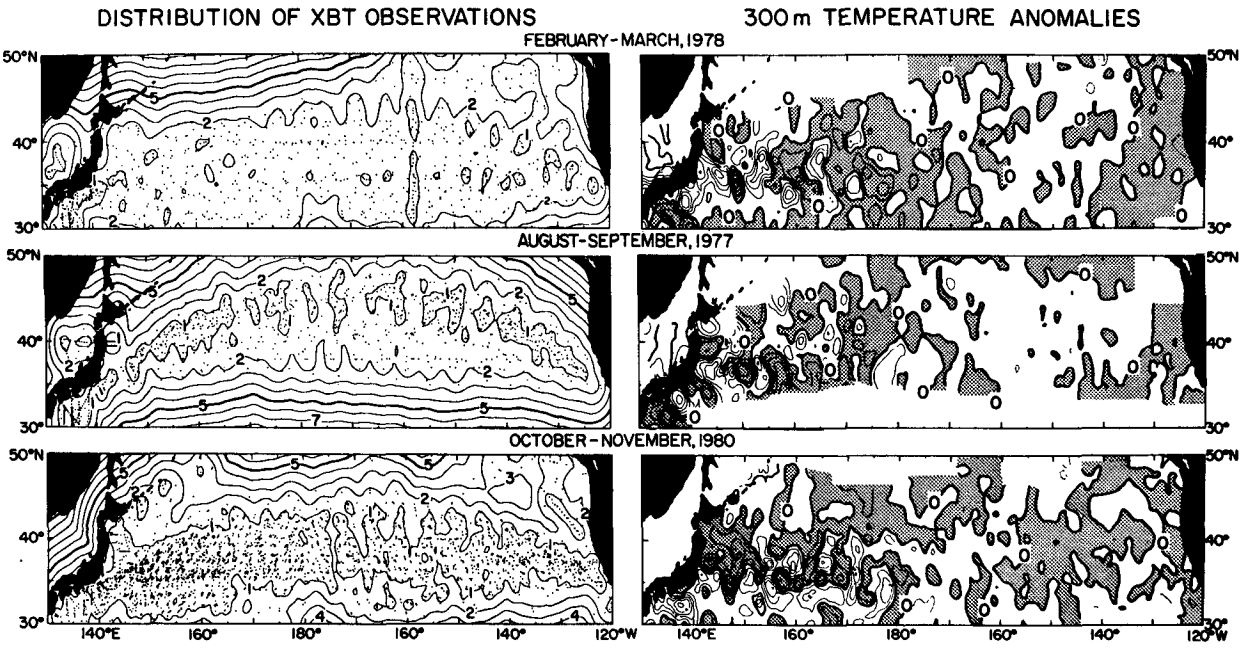

FIG. 2. (a) Distribution of XBT observations for three bimonths, corresponding to months of poor-to-average sampling (Feb–Mar 1978; 961 samples), average sampling (Aug–Sep 1977; 1016 samples) and good sampling (Oct–Nov 1980; 3203 samples). Dots show the observation points; contours are the average distance to the eight nearest observations from each ½° grid point, in degrees of latitude/longitude. (This distance is about 20% larger than the separation of nearest-neighbor observations.) (b) Anomalous temperatures at 300 m for the same three bimonths with mean and annual cycle removed (1°C contours).

positions and corresponding $\bar{r}_8$ for three bimonths chosen to typify poor, average, and good coverage. The last was during an intensive observation period in 1980 and represents the best coverage available. These three bimonths also illustrate the seasonal migration of shipping lanes and densest sampling. As remarked before, the contoured quantity ($\bar{r}_8$) is the average distance in degrees to the nearest eight points from each ½° grid point. Degrees in latitude and longitude were treated identically on these maps and also for all wavenumber spectra. Examination of these maps and of maps of $\bar{r}_8$ for all 48 bimonths shows relatively few values beyond the 2° contour even though S2 interpolates temperatures to grid points where $\bar{r}_8$ is as large as 4° or 5°. Therefore, only regions where $\bar{r}_8$ is less than 2° are used in this study. This means that the number of realizations in each averaged wavenumber spectrum is generally less than 48 (the total number of bimonths) and depends strongly on latitude or longitude. It is also not possible to form complete time series at all grid points. Waves shorter than 3.3° will be aliased; how much energy is aliased and to which wavelengths requires further tests because of nonuniform data density and locally random observation locations.

Three maps of anomalous temperature at 300 m (Fig. 2b) illustrate the effect of different observation densities on mapping the temperature field. With a resolution ($\bar{r}_8$) of about ½° latitude/longitude (October–November 1980), the shape of the eddy field is clearly much better resolved than with the 1° or 2° sampling of the other two maps, although the *presence* of eddies is fairly well resolved by all maps. (By "eddies" are meant temporal variability; in the present context, we are referring to energetic features with small spatial scales.) This reflects the decorrelation scale of about 200 km (Koblinsky et al., 1984). Visually, the increase in resolution to ½° improves the finer details of eddy shapes and perhaps the magnitude of the eddies.

Because the data distribution is locally random and because its density varies in space, empirical tests were used to determine the form that aliasing takes. This was done by sampling individual plane waves by the observed XBT positions, gridding the resulting data, and computing the associated two-dimensional spectrum. The distribution of data, the S2 gridding procedure, and the spectral method all combine to filter the actual temperature variability; in order to determine the response function of this filter, random numbers were assigned to each XBT position and were then processed in exactly the same manner as actual temperature anomalies. The aliasing and filtering tests are described in the Appendix. The results can be summarized as follows: 1) wavelengths longer than 3° or 4° are not aliased, 2) shorter waves are partially resolved and are smeared to longer wavelengths although a peak is still found at the input wavelength, and 3) the S2 procedure is a low-pass filter with an averaging radius of approximately 2° when regions with $\bar{r}_8$ less than 2° are used. The first result indicates that the effective Nyquist wavelength is indeed associated with the worst average spacing between observations. As a consequence of the second result, a grid with ½° spacing (corresponding to the best-observed resolution) is a better choice than a 2° grid (corresponding to the worst-allowed resolution) in order to partially resolve wavelengths of 1° to 4° and hence reduce the amount of aliasing.

Because the oceanic temperature spectrum is inherently red and because S2 artificially reddens the spectrum, some previous analyses have employed a filter to explicitly study the shorter mesoscale waves without leakage from the dominating larger scales (White, 1982; Kang and Magaard, 1980). The high-pass, mesoscale filter that was used is the difference between temperature anomalies and their spatial average in a 4° latitude by 10° longitude box about each ½° grid point. The response function of the mesoscale filter is

$$\left|1 - \frac{\sin(2\pi k L_x)}{2\pi k L_x}\,\frac{\sin(2\pi l L_y)}{2\pi l L_y}\right|^2$$

where L_x and L_y are the box half-widths. With (L_x, L_y) of (2°, 5°), the filter has minima at 4° on the k-axis and at 3.3° on the l-axis, and off-axis at (6.67°, 2.67°). When combined with S2, which filters out most wavelengths shorter than 3°, the filtering passes a narrow band from about 3° to 4° in the meridional direction and 3° to 10° in the zonal direction. It is a rather "lumpy" band-pass filter and we have decided not to use it.

4. Observed temperatures

In this section are presented the eight-year mean and standard deviations of the 300 m temperature, its mean annual cycle, and its residuals after the long-term mean and annual cycle were removed.

A two-month time bin was chosen for gridding in order to improve spatial resolution. This choice was discussed before. An obvious difficulty arising from this choice is that some events in the Kuroshio Extension (such as ring formation) occur over time scales shorter than a month. Therefore, we will not be able to resolve these higher-frequency, but still important, processes in the temperature fields. Comparison of our sequence of bimonthly maps with Koblinsky et al.'s (1984) monthly maps and Bernstein and White's (1981) monthly maps (none of which are shown) indicates that where sampling is dense, events can be followed more easily with time bins of one month. However, spatial sampling in one-month segments was much patchier than in two-month segments. Events are much more difficult to follow with three-month bins used by White (1982) and Mizuno and White (1983), as they pointed out. Qualitative examination of the one-month, two-month, and three-month temperature anomalies shows that, although extrema are lessened

with longer time bins, eddy scales are not degraded, reflecting the essential redness of the spectra.

a. Long-term mean and standard deviation

The long-term mean temperatures at 300 m from the eight years of XBT observations are shown in Fig. 3, along with the rms differences about the long-term mean. The mean is an average of individual bimonthly temperatures which were mapped to a ½° grid using S2. The average sampling density for each bimonth does not warrant ½° resolution over most of the North Pacific, but this finest sampling is shown here because local sampling density is high in some areas, especially where shipping lanes converge. The actual resolution of a given bimonthly map in the Kuroshio Extension region is better than 1°, reflecting the smoothing scale of S2 given the average local sampling density as discussed in the previous section.

The mean temperature shown here is qualitatively similar to that shown in Mizuno and White (1983), using the first four years of TRANSPAC XBT data. The field is also similar to the mean geopotential anomaly map of Hasunuma and Yoshida (1978). The major features, although somewhat smoother here, are essentially unchanged from those observed in earlier studies. The Kuroshio Meander at 137°E is well resolved in the mean; during the 8 years it was absent only from October 1980 to September 1981, although it was weak throughout 1980 (White and He, 1986). Two meanders of the Kuroshio Extension, with ridges at 144° and 150°E, are also present. The location of the first meander at 144°E is a common site for warm-core ring formation (Kawai, 1972; Kitano, 1975). Ring spawning at the 150°E meander is less clear, although Kitano mentions a few occurrences of rings there; Mizuno and White (1983) track several warm and cold core rings found at about 150°E. The mean, zonally directed isotherms spread meridionally in marked fashion at 156° and 164°E; both phenomena were discussed in Mizuno and White (1983). The spread at 156°E is just west of the Shatsky Rise (160°E) and results from the bimodal path of the Kuroshio which tends to flow either north or south of Shatsky Rise; it is not due to a bifurcation of the current there. However, the spread at 164°E, between the Shatsky Rise (160°E) and the Emperor Seamounts (170°E), *is* due to a bifurcation of the Kuroshio Extension (Levine and White, 1983). Further splits of the Kuroshio Extension east of Emperor Seamounts were shown by Levine and White (1983) but are not easily discerned from this mean temperature map.

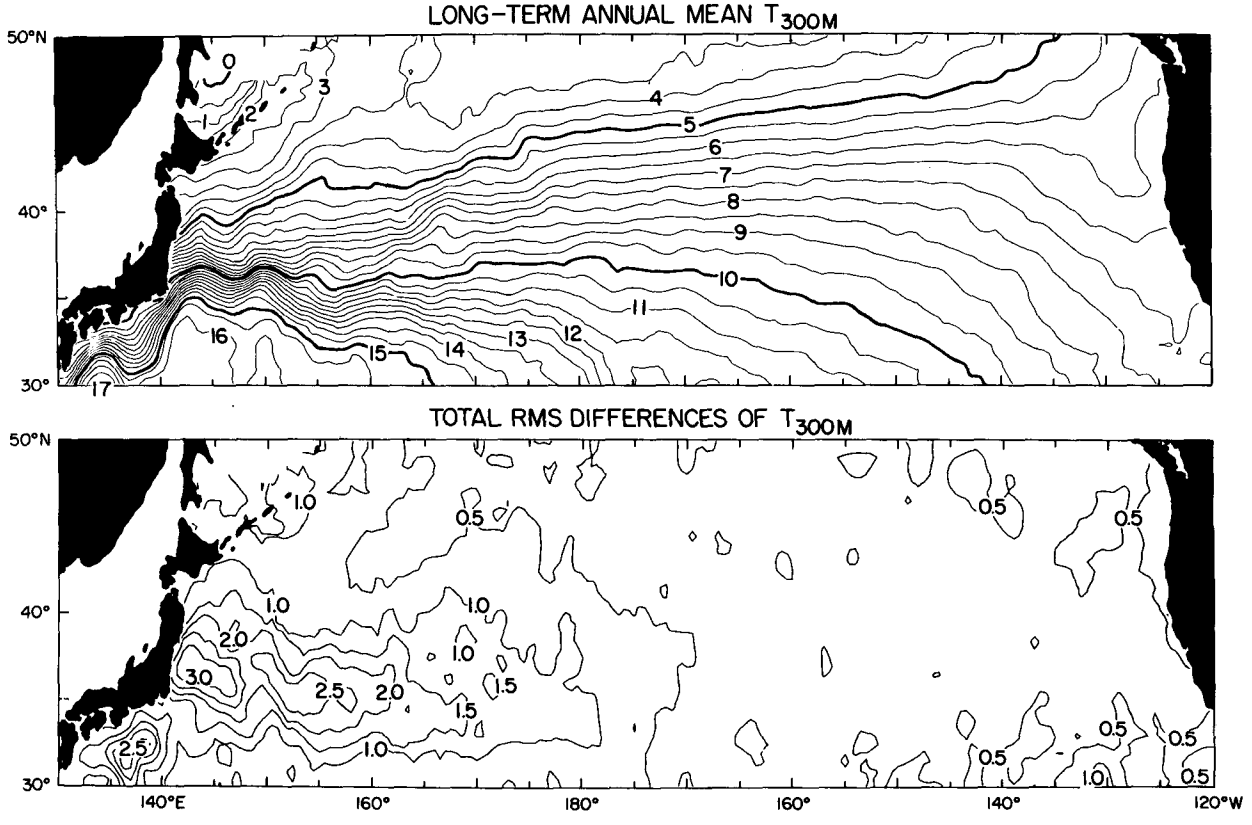

FIG. 3. (a) Long-term mean temperatures at 300 m using all observations shown in Fig. 1. (b) Root-mean-square differences of 300 m temperature about the mean. Both figures were plotted using a ½° grid.

A feature not specifically noted before is intensification of the temperature gradient associated with northward shear flow in the Kuroshio at 133°, 142° and 148°E. We do not have a ready explanation of this observation. Various possibilities have been tried and rejected, including eastward decay of the meandering current, tilting of the background temperature field relative to the direction of the Kuroshio Extension, nonlinear steepening of the meanders, and conservation of potential vorticity including relative vorticity, planetary vorticity, stream curvature and stretching.

The rms differences of the bimonthly 300 m temperatures about the 8-year mean are shown in Fig. 3b. Details of a similar distribution in the Kuroshio region were discussed by Mizuno and White (1983) using 3-month averages. The main point we reiterate here is the dramatic six-fold decrease in rms differences between 160°E and 170°W at the latitude of the Kuroshio Extension. East of 170°W, variance is nearly constant, increasing only slightly at the eastern and southern sides, reflecting increased variability and/or poorer sampling. The enormous change in variance between 160°E and 170°W has led us to divide the North Pacific at 170°W into western and eastern regions for analysis in section 5. West of 160°E, rms differences are highest in the Kuroshio Extension, with a six-fold decrease north and south of the current. Particularly high rms differences are found in patches along the Kuroshio Extension, corresponding to ring-producing locations; these locations also coincide with ridges in the quasi-stationary meanders at 144° and 150°E.

Division of the total rms differences shown in Fig. 3b into the part due to the annual cycle and that due to anomalies about the annual cycle is not shown here because it has been discussed in earlier studies. In Mizuno and White (1983), the total sample variance of 300 m temperature in the Kuroshio Extension region was shown to be associated principally with anomalous variability (estimated to be 70%–80% of the total), with little due to the annual cycle. It was demonstrated, however, that anomalous variance in winter was twice as large as in summer, an observation exploited by White and He (1986) in their further determination that mesoscale patterns in the Kuroshio Extension tended to be quasi-stationary throughout most of the year, changing in winter. In White (1982), the total sample variance of 300 m temperature in the eastern midlatitude Pacific also was shown to be associated principally with anomalous variability (estimated to be 50%–75% of the total), with little due to the annual cycle. Both of these studies yield results that are qualitatively similar because the wavenumber/frequency spectra are red, which is to be demonstrated in the present study.

b. The mean annual cycle

The average annual cycle over the 8 years was computed by averaging each group of eight bimonths (December–January, February–March, etc.) together. The resulting long-term bimonthly mean maps in the Kuroshio Extension region are only slightly different from the seasonal averages shown in Mizuno and White (1983), although there are now eight realizations in each average rather than four. For this reason, maps for each bimonth are not shown here, but they are discussed in the context of the map of the total 8-year mean shown in Fig. 3a. In the 8-year mean, the Kuroshio Meander at 137°E was pronounced in all bimonths and similar to the long-term mean (Fig. 3b) except in April–May when it was virtually absent. The two Kuroshio Extension meanders at 144° and 150°E are present in most bimonths. However, the first meander was muddled or absent in December–January, while the second meander was quite weak in April–May. In contrast to Mizuno and White's (1983) findings, there was no pronounced seasonal change in distance between the ridges of these two meanders; the distance was always 5.5° to 6° longitude or about 540 km. A third meander (i.e., a ridge) was present at 154°E from February to May. In all bimonths, the Kuroshio Extension east of 140°E flowed southeastward, forming a trough at about 155°E, similar to what is seen in the long-term mean (Fig. 3a). This creates the "spread" in mean isotherms at 155°E. A weak spread in the 300 m isotherms always occurs in the region 162°–168°E and therefore is found in the long-term mean. There is a reorganization to more compressed isotherms at about 170°E, the location of the Emperor Seamounts. In the eastern North Pacific the annual cycle is much weaker than in the west; there is a slight southward displacement of isotherms in winter north of the 8°C mean isotherm, corresponding to a change of 0.1°C locally.

The time/longitude and time/latitude matrices (Figs. 4 and 5) of the annual cycle of 300 m temperature, with the overall long-term mean removed, display zonal and meridional propagation. The time/longitude matrix at 40°N is plotted in the upper panel of Fig. 4, with three cycles repeated. The dominant signal is long bands of nearly zonally uniform highs and lows broken only by a region of strong westward propagation between 165°E and 180°. Closer examination of the long bands shows that the coolest bimonth at all longitudes is February–March or April–May. However, only east of 150°W is the warmest bimonth (August–September) predominantly during the summer; in the western and central Pacific, the warmest bimonth is during October–November or December–January. The 300 m surface lies well below the seasonal mixed layer so that horizontal advection, vertical diffusion (White and Bernstein, 1980), and Ekman pumping (White et al., 1980), are important processes. East of 180°, short-scale features (600 km wavelength) are superimposed on the nearly zonally uniform signal; they tend to propagate westward at about 3 cm s^{-1}. [White (1977) found that the detection of annual, baroclinic, long,

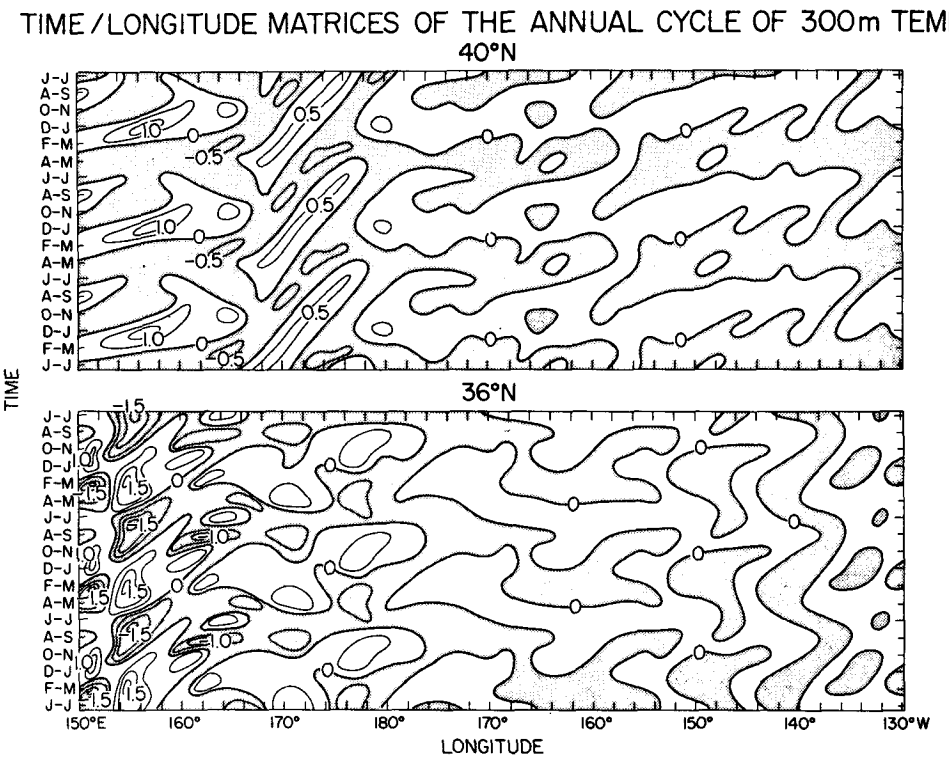

FIG. 4. Annual cycle of temperature at 300 m (long-term mean removed), displayed as a time–longitude matrix at 36° and 40°N. Plotted using a 2° grid. Time increases downward. Each annual cycle is repeated three times for display purposes.

(Rossby) waves was enhanced by subtracting the zonally uniform portion of the annual cycle.] Between 165°E and 180°, westward propagation dominates. In the westernmost region, there might be eastward propagation at 4 cm s^{-1} superimposed on a westward-propagating signal which could be part of the bands found east of 180°; westward propagation is approximately 9 cm s^{-1}.

The time/longitude matrix of the annual cycle of 300 m temperature at 36°N is plotted in the lower panel of Fig. 4, again with three cycles shown. The annual cycle is much less zonally uniform east of 155°E than at 40°N, with more short-scale features which propagate both westward and eastward. The apparent eastward propagation is well resolved and is not an artifact of the procedure. It might be forced directly by eastward propagation in the overlying annual cycle in the wind stress curl, or it might result from eastward advection associated with the North Pacific Current. West of 165°E, there is westward propagation at speeds of approximately 4–5 cm s^{-1}, somewhat faster than found at 40°N, as expected from the long-wave dispersion relation for baroclinic waves assuming that the deformation radius is the same at both latitudes. (The physical regimes are also entirely different: the Kuroshio Extension dominates the western Pacific at 36°N.)

The time/latitude matrices of the annual cycle of 300 m temperature at 150°E and 150°W are plotted in Fig. 5. The largest magnitude at 150°E is at 37° to 38°N, somewhat farther north than the largest values of rms differences for the overall dataset (Fig. 3b): largest variability in the annual cycle occurs in the region between the Kuroshio Extension and the Oyashio Extension, the so-called "mixed water" region. At 150°E, propagation tends to be away from the large amplitudes found at the axis of the Kuroshio Extension; phase speeds appear to be 3 to 6 cm s^{-1}.

We can attempt to link this propagation in the annual cycle with Rossby waves; on the other hand it may be associated with advection by a seasonally varying gyre. To explore the linkage to Rossby waves, consider what would happen if the Kuroshio Extension were the source of variability in the region: for free Rossby waves, meridional phase and group velocities are oppositely directed so the signature of an energy source at the Kuroshio Extension would be phase velocities directed *toward* rather than away from the current. However, it can be easily shown that in the presence of eastward flow, phase and group velocity can be in the same direction, depending on the magnitude of the flow. Therefore, the observation of phase propagation away from the Kuroshio Extension does not indicate conclusively that the Kuroshio Extension is not a source of variability for the adjacent regions to

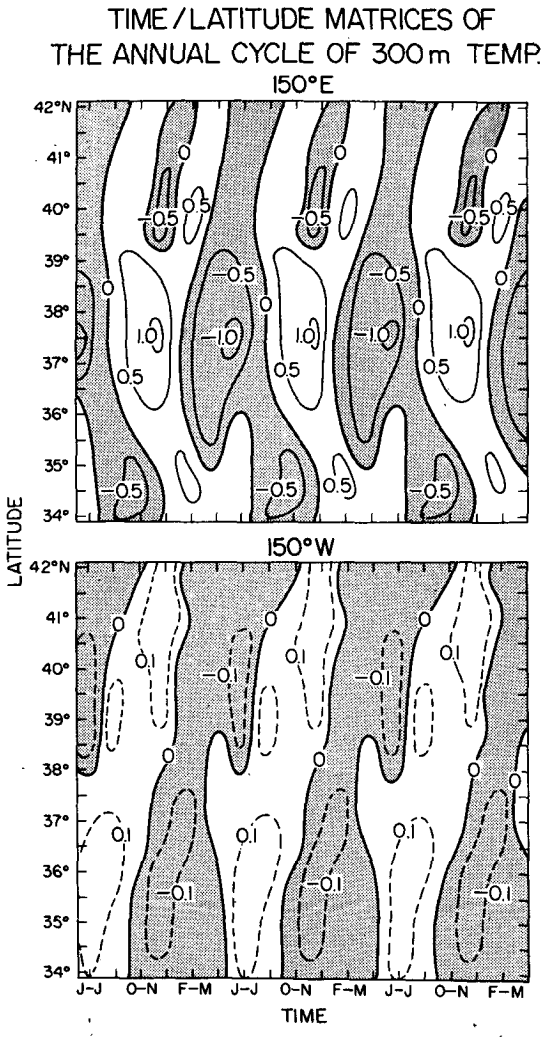

FIG. 5. Annual cycle of temperature at 300 m (long-term mean removed), displayed as a time–latitude matrix at 150°E and 150°W. Plotted using a ½° grid. Each annual cycle is repeated three times for display purposes.

the north and south. In fact, if a broad eastward flow exists on either side of the Kuroshio Extension, so that phase and group velocities are in the same direction, this would be evidence that the annual cycle in the Kuroshio Extension *is* a source of variability for the adjacent regions to the north and south.

In the east (150°W) a tendency exists for northward propagation at approximately 4–5 cm s^{-1}. This northward speed, coupled with the westward speed of 3–4 cm s^{-1} observed at 40°N, indicates a wavevector directed toward the northwest, consistent with observations of Kang and Magaard (1980). White and Saur (1981) hypothesized northwestward phase propagation when zonally traveling baroclinic waves generated in the east are refracted northward by the poleward decrease in zonal phase speed of the long baroclinic waves, due both to the northward increase of f and to the shallowing of the main thermocline.

c. *Anomalous 300 m temperatures*

Anomalous temperatures at 300 m were computed by subtracting the 8-year mean and annual cycle from observed temperatures at each grid point. These anomalies form the basic dataset for spectral calculations in the next section. Three maps of anomalous temperature at 300 m were shown in Fig. 2b. The largest anomalies occur in the Kuroshio Extension region, consistent with largest variance about the long-term mean found there (Fig. 3b). Within the Kuroshio Extension, the most energetic features are at the positions of the meanders which appear in the long-term mean (Fig. 3a). When the anomalous temperature is divided by the rms differences about the time mean at each grid point, a clear change from shorter zonal length scales in the west to longer scales in the east is seen.

Time/longitude matrices of 300 m temperature anomalies at 40° and 36°N for the midlatitude North Pacific from 150°E to 130°W are displayed in Fig. 6. The magnitude of the anomalies is relatively uniform over the eastern and central portions from 180° to 130°W; west of 180° the magnitude increases, much more at 36° than at 40°N because of the presence of the Kuroshio Extension near 36°N (Fig. 3a). The anomalies in the Kuroshio Extension are much larger than those of the annual cycle (Fig. 4), consistent with the results of Mizuno and White (1983). Both time/longitude matrices are noisy but display a tendency for westward propagation which we roughly estimate from these figures to be 3 cm s^{-1}. There is also an overall temporal trend, especially at 40°N and in the eastern Pacific, from warmer than normal values during the first half of both records to colder than normal values during the second half, with a net cooling of about 1°C. In the Kuroshio Extension (at 36°N west of 180°), both westward and eastward propagation can be seen, but westward propagation clearly dominates. Time and space scales of anomalies in the Kuroshio Extension are smaller than those east of 180°, but with qualitatively similar propagation speeds. At 40°N, the time and space scales are more nearly uniform over the entire space domain, although a tendency towards smaller scales exists west of 180°. This will be demonstrated quantitatively in the frequency/zonal wavenumber spectra in the next section.

Latitude/time matrices of 300 m temperature anomalies at 150°E and 150°W (Fig. 7) also show large amplitudes in the Kuroshio Extension compared with regions to the north, south, and east. The Kuroshio Extension appears to have shifted from about 37°N in the first half of the record to 36°N in the latter half, based on the latitude of the largest anomalies. At 150°E there is very weak evidence of northward (southward) propagation north (south) of the Kuroshio Extension

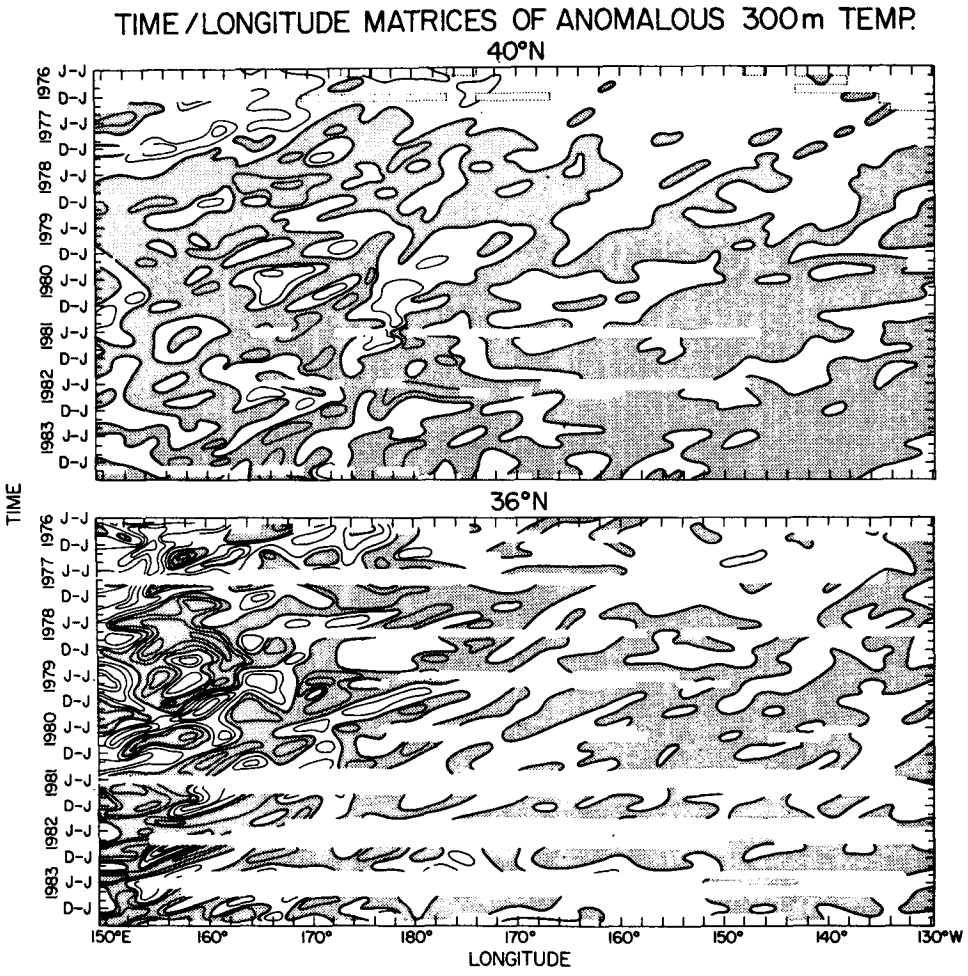

FIG. 6. Anomalous temperature at 300 m (bimonthly means removed) as a function of longitude and time at 40° and 36°N. Plotted using a 1° grid. Shaded areas are negative. The contour interval is 1.0°C. Areas where $\bar{r}_8$ was greater than 2° are blank.

in the first half of the record (1976–80). Clearer propagation away from the axis of the Kuroshio Extension occurs in the annual cycle (Fig. 5). The dominant patterns in both matrices are north–south contours; anomalies seem to occur almost instantaneously at all latitudes. Because of the two-month time bin and limited latitude range, we can detect only patterns with meridional phase speeds less than 10 cm s^{-1}, which is the speed for covering 6° of latitude in two months. If the field is dominated by first-mode baroclinic Rossby waves with internal deformation radii of 20 to 100 km and zonal wavelengths of 500 to 3000 km, only waves with meridional wavelengths less than 100 to 200 km propagate more slowly than 10 cm s^{-1} in the meridional direction. However, wavelengths less than 300 to 400 km cannot be resolved adequately at all latitudes given the average XBT sampling density. Therefore, first-mode baroclinic Rossby waves which can be resolved spatially (longer than 300 km) will appear to propagate instantaneously in the meridional direction (faster than 10 cm s^{-1}) while the waves which move slowly enough so that their direction of propagation can be determined will not be resolved spatially.

An overall trend occurs at 150°W from anomalies which are positive (warmer) at the start of the record to negative (colder) in the latter part. This trend is apparent in sea-surface temperature anomalies for the northeastern Pacific (Namias, personal communication) and may result from an intensification of the Aleutian Low. Fluctuations which appear at both 150°E and 150°W have no set periodicity, varying from about 6 to 16 months.

5. Spectra of anomalous 300 m temperatures

Wavenumber and frequency spectra were computed for the normalized temperature anomalies at 300 m. Recall that temperatures were grouped in bimonths and gridded every ½° latitude/longitude. Only data from more adequately-sampled regions were used, as

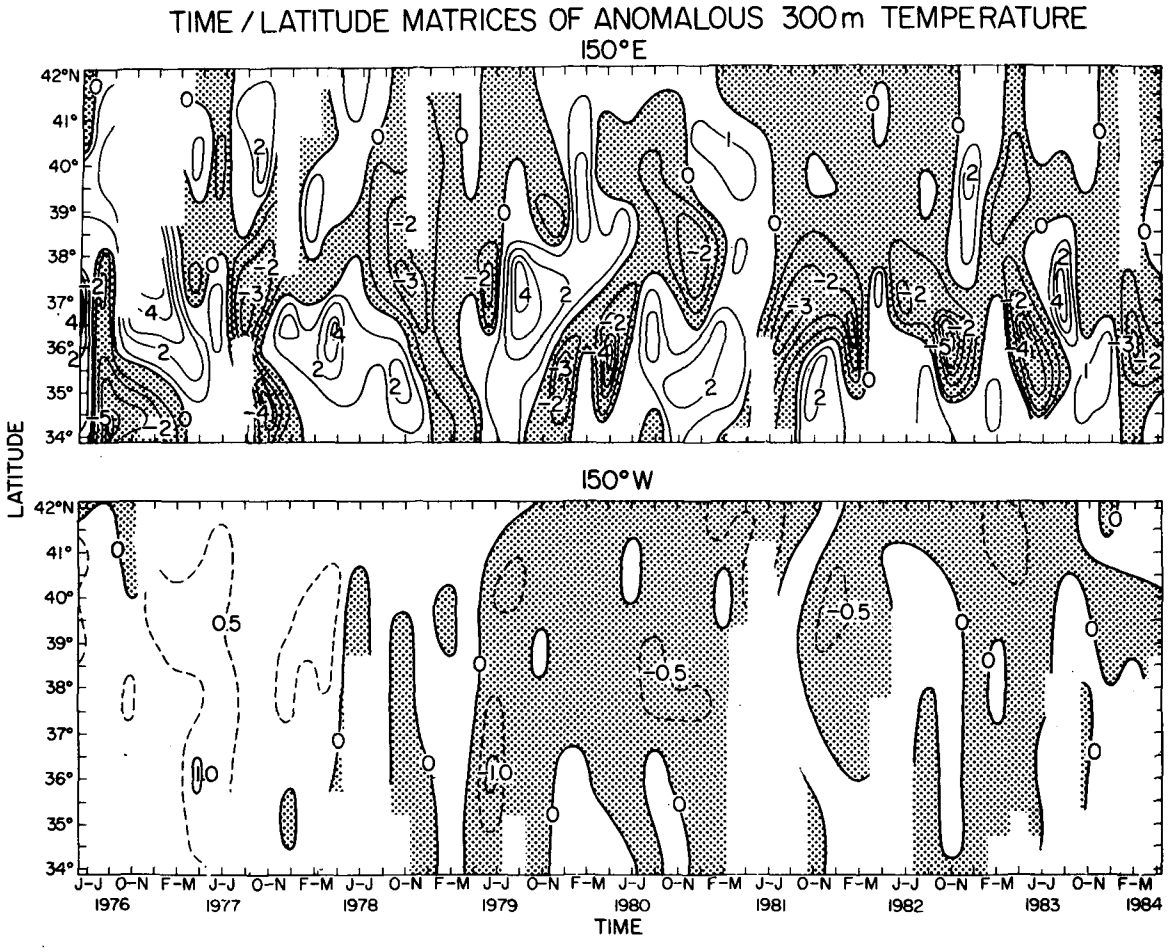

FIG. 7. Anomalous temperature at 300 m (bimonthly means removed) as a function of latitude and time for 150°E and 150°W. Plotted using a 1° grid. The contour interval is 1°C at 150°E and 0.5°C at 150°W. Areas where $\bar{r}_8$ was greater than 2° are blank.

defined by the criterion that $\bar{r}_8$ be less than 2° latitude/longitude (section 3). One-dimensional zonal wavenumber (k) and frequency (ω) spectra, and two-dimensional ω/k and k/l spectra are shown. Meridional wavenumber (l) spectra are not shown because they add little useful information, the record lengths being very short owing to the geometry of the gyre and the dataset. In addition, ω/l spectra were not computed because it was not possible to form a continuous time series with adequate spatial coverage at any longitude; based on the discussion of Fig. 7 in the preceding section, we would expect these spectra to be extremely red in meridional wavenumber if they could be computed. On the other hand, there were a number of individual bimonths with adequate spatial coverage to form k/l spectra; these are shown because they contain directional information even though the series are quite short in the meridional direction.

For construction of all spectra, the midlatitude North Pacific was divided into a western region (150°E to 170°W) and an eastern region (170° to 130°W) based on the rms differences of 300 m temperature shown in Fig. 3b, which shows a region of large variance in the Kuroshio Extension and lower variance in the eastern North Pacific. The zonal contrast in variance from west to east across the North Pacific at the latitude of the Kuroshio Extension is well known (Bernstein and White, 1977; Fu, 1983, among others) and is associated with eddy activity; synoptic zonal temperature sections across the central Pacific, as displayed in Bernstein and White (1977), show an abrupt change at about 175°W. We considered dividing the North Pacific into three regions, with an additional boundary at 160°E separating the uniformly high eddy activity of the Kuroshio Extension from a region where the variance drops steadily to the east to 170°W. For spectra, however, we wish to have the longest possible records without sacrificing statistical homogeneity; hence we assume that space scales typical of the Kuroshio Extension extend to 170°W, the easternmost point of enhanced eddy activity associated with the current.

Inhomogeneity and nonstationarity are problems in

the vicinity of the Kuroshio Extension because length and time scales and energy levels differ in and outside the Extension. As the Kuroshio Extension is displaced meridionally past a set of grid points, the temperature structure which is being sampled at the points could change its statistical characteristics. There is no way to compensate for this true inhomogeneity and nonstationarity. However, we have attempted to compensate for the type of inhomogeneity due to the spatially varying energy distribution by normalizing data at each point by the standard deviation from the time mean at that point. This normalization levels the spatial distribution of total variance so that a wavenumber spectrum based on a line of data which crosses from a high-variance to a low-variance region will not be weighted towards events which occur in the region of highest variance. Also, since a large number of spectral realizations are averaged to improve reliability, the final average is not weighted towards those bimonths or positions which have higher spectral energy.

a. Zonal wavenumber spectra

Wavenumber spectra of subsurface temperature in the midlatitude North Pacific have been discussed by a large number of previous investigators. Our treatment adds little new information, and indeed utilizes a dataset with somewhat poorer resolution, but is useful as a summary of variations in length scales across the Pacific and as a prelude to the discussion of two-dimensional ω/k and k/l spectra. Various investigators have used synoptic XBT and hydrographic sections with observations spaced no more than 80 km apart (Bernstein and White, 1974, 1977, 1982; Wilson and Dugan, 1978), and SEASAT data with effective resolution of about 100 km (Fu, 1983). The main results of previous works were: 1) fairly flat spectral energy density for wavelengths longer than 250 km with occasional peaks in the 500 to 1000 km range which may have been due to detrending (Bernstein and White, 1974, 1977; Wilson and Dugan, 1978; Fu, 1983); 2) a drop in spectral energy density for wavelengths shorter than 250 km; 3) shorter dominant scales in the Kuroshio Extension (Koblinsky et al., 1984; Harrison et al., 1983; Wilson and Dugan, 1978) and in the west compared with the east (Fu, 1983); and 4) higher spectral energy density in the Kuroshio region.

We have used a gridded version of a much larger XBT dataset which labels as "simultaneous" all observations within a two-month time span. Clearly, some information is lost near the effective Nyquist wavelength, which was shown in section 3 to be 3° to 4°, since the corresponding decorrelation time scale is one to two months, at least in the Kuroshio Extension region (Koblinsky et al., 1984). However, since the gridded data are also used for two-dimensional spectra, it is important to establish how well the one-dimensional spectra perform.

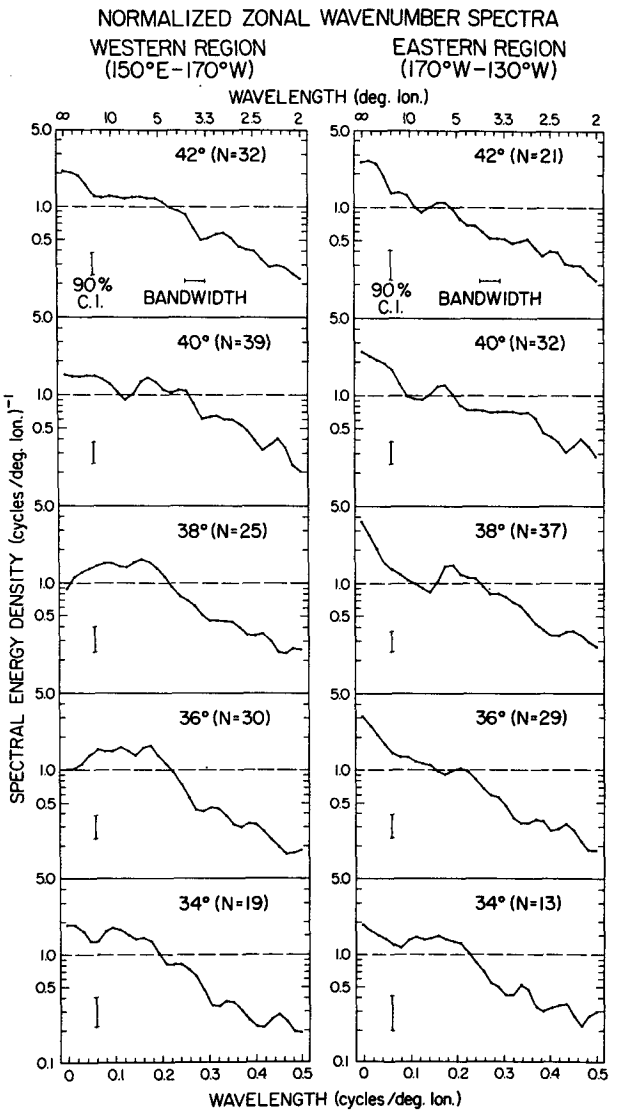

FIG. 8. Zonal wavenumber spectra for (a) western midlatitude North Pacific (150°E–170°W) and (b) eastern North Pacific (170°–130°W) at 34°, 36°, 38°, 40° and 42°N. The number of realizations in each averaged spectrum is indicated. Only wavelengths longer than 2° are shown although data were gridded at ½° intervals: the effective Nyquist wavelength based on actual sampling density is between 3° and 4°.

Zonal wavenumber spectra for the midlatitude western North Pacific (150°E–170°W) and midlatitude eastern North Pacific (170°–130°W) are shown in Fig. 8. The ½° space series were used, bearing in mind that actual resolution is ½° to 2°. Only space series for which $\bar{r}_8$ was less than 2° at all points were used. First, each data value was normalized by dividing by the standard deviation about the time mean at its grid location. Each space series was linearly detrended and the standard Blackman–Tukey method was applied, with spectra computed as the squared Fourier transform of the windowed autocorrelation function. A Tu-

key lag window of 62 lags was used. Spectra shown in Fig. 8 are ensemble averages of 13 to 40 bimonthly realizations, each computed with 3 to 4 equivalent degrees of freedom. After averaging, the total number of degrees of freedom ranged from 44 to 136. [Because the decorrelation time scale is about one month (White and Bernstein, 1979; Koblinsky et al., 1984), each spectrum in the average was assumed to be independent although the number of degrees of freedom for the longest waves, which also have long time scales, may be much less.] Finally, each averaged spectrum was divided by the response function discussed in the Appendix: the response function is the average spectrum of random numbers assigned to actual data points and subjected to precisely the same procedures as the data. Because the spectra are normalized in space and time, they obviously do not illustrate the enormous increase in spectral energy density towards the Kuroshio Extension region; this has been amply demonstrated (Bernstein and White, 1977) and is clear from the rms differences shown in Fig. 3b.

All spectra shown in Fig. 8 are obviously red overall. Attention should be focussed only on wavelengths longer than 3°; since the grid spacing is ½°, wavelengths as short as 1° can be calculated (and are shown to 2°) but actual data coverage was coarser than ½°, as discussed previously. Significant differences between the spectra emerge at longest wavelengths. Eastern Pacific spectra peak strongly at the longest wavelength; there is also a statistically significant second peak at about 5° wavelength at 38°N with a tendency towards this peak at other latitudes. Western Pacific spectra do not peak at the longest wavelength; as the Kuroshio/Oyashio Extension region is approached, the spectra broaden towards shorter scales. Spectra at 36°N, 38°N and 40°N are broadest. The half-power point is also shifted significantly to shorter wavelengths in the Kuroshio/Oyashio spectra compared with the eastern Pacific spectra.

The robust, important feature of these spectra is that the dominant, energy-containing portion of the western Pacific spectra shifts to shorter wavelengths as the Kuroshio/Oyashio Extension region is approached. Because of aliasing and resolution, the shape of the spectral rolloff is not reliable; the precise shape of the longwave spectrum is probably also affected. However, the existence and position of peaks is probably correct within the limits given by the bandwidth and confidence intervals since aliasing tests indicate that energy associated with short wavelengths is smeared out rather than placed in false peaks.

b. Frequency spectra

The frequency spectrum of temperature and velocity in the upper waters of the midlatitude North Pacific is known in a few places as a result of long-term moorings and weather stations. Previous studies suffer from short series length, a shortcoming which appears at first glance to be overcome for the mesoscale in the TRANSPAC dataset. However, frequency spectra that are presented here suffer from poor spatial resolution of ½° to 2° and the corresponding temporal resolution of two months. Because we use average spectra from a range of longitudes in the western and eastern North Pacific in order to increase the degrees of freedom, we do not take advantage of denser XBT sampling in more limited regions where it would be possible to use smaller time intervals. Our Nyquist period of 120 days is clearly marginal based on previous analyses of time scales (e.g., Koblinsky et al., 1984).

Frequency spectra for the western (150°E–170°W) and eastern (170°–130°W) North Pacific at 36° and 40°N are shown in Fig. 9. Each spectrum is an ensem-

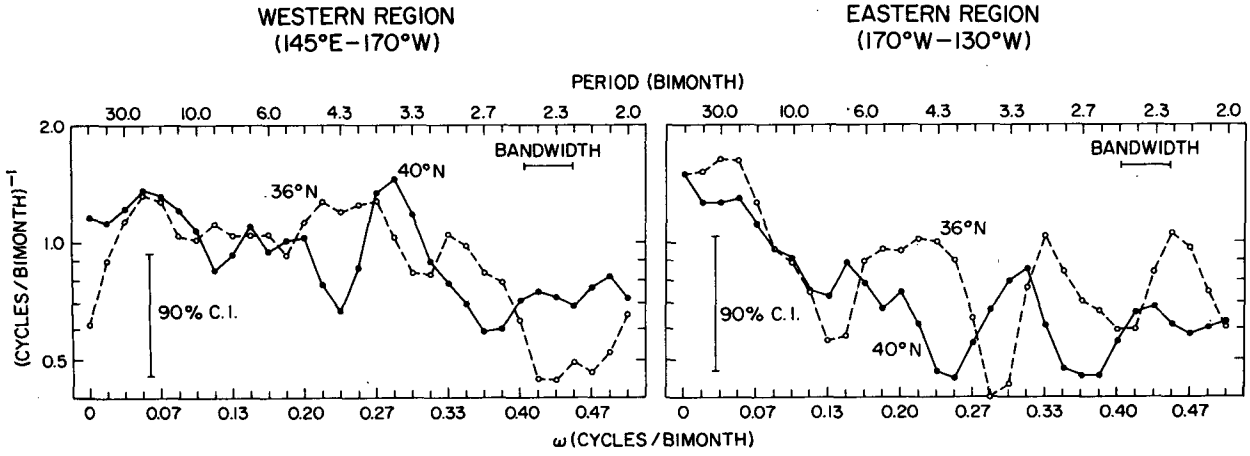

FIG. 9. Frequency (ω) spectra for (a) western North Pacific (150°E–170°W) at 36° and 40°N and (b) eastern North Pacific (170°–130°W) at 36° and 40°N. Each spectrum is an average of spectra formed every 5° along the labelled latitude; thus there are nine realizations for the western and eight realizations for the eastern Pacific spectra.

ble average of spectra formed every 5° of longitude in the specified longitudinal band; for example, the spectrum at 36°N in the western Pacific (145°E–170°W) is an average of 10 spectra. As with the wavenumber spectra, spatial sampling in all bimonths used was required to be reasonable ($\bar{r}_8$ less than 2°). At 40°N, the average number of bimonths used for the spectra at each longitude was 46 of a maximum possible of 48, with a range of 43 to 47. Due to the latitudinal seasonal migration of shipping lanes, observational coverage at 36°N was not as thorough as at 40°N; the average number of bimonths used was 38 (out of 48), with a range of 31 to 48. Most missing bimonths at 36°N were in summer. All data were normalized by the standard deviation about the time mean at each spatial grid point. Obviously this does not affect the spectrum at a given point, but it does mean that each spectrum in the average is weighted equally. Time series were detrended and a Tukey lag window with 30 lags was used. Each spectrum was divided by the response function shown in the Appendix. The average number of degrees of freedom for individual spectra was 8 to 9 for the western Pacific and 7 to 8 for the eastern Pacific. Total degrees for the ensemble-averaged spectra in the western and eastern Pacific were 86 and 65, respectively.

All frequency spectra are fairly white with a small, but significant, decrease in energy with increasing frequency. This whiteness is not surprising considering that our Nyquist period is 120 days. The large troughs at 4, 6 and 12 months, which are evident in the response functions shown in the Appendix, are nearly eliminated from these spectra although their presence is still felt at 36°N in the eastern Pacific where the troughs do not occur at exactly 6 and 12 months. There is a slight difference between the western and eastern Pacific spectra: spectra from the east are somewhat redder, especially at 40°N where there was an overall cooling trend, as remarked previously. Two-dimensional ω/k spectra shown in the next section elucidate the differences between western and eastern Pacific spectra.

c. *Frequency-zonal wavenumber (ω/k) spectra*

The methods outlined in the previous sections were used to compute normalized frequency-zonal wavenumber ω/k spectra at 36° and 40°N in the western (150°E–170°W) and eastern (170°–130°W) North Pacific. There were not enough data at more extreme latitudes (e.g., 32°N) for ω/k spectra. All points were divided by the standard deviation about the time mean at each spatial point. Each zonal series and then each time series was detrended. The resulting time/longitude matrix was further detrended using a plane fit (Pierson, 1960), although most of the trend was removed in the first process. Spectra were computed as a two-dimensional Fourier transform of the time-longitude autocorrelation matrix using Pierson's (1960) Tukey-like window with 30 lags in space and 16 lags in time and then normalized by the standard deviation about the mean of the matrix. Since there is only one realization of each ω/k spectrum, no additional ensemble-averaging was possible. (We did not wish to assume that data at neighboring latitudes was independent or, if it was independent, that the statistics were the same.) Each spectrum has 11 degrees of freedom, based on Pierson's (1960) expression for two-dimensional spectra using this lag window.

The ω/k spectra are shown in Fig. 10 and are easy to interpret. In all four spectra, most spectral energy density is in the left-hand quadrant; hence propagation is more westward than eastward at all four locations at a phase speed of 2 to 3 cm s^{-1}. Significant eastward propagation (at about 0.5 cm s^{-1}) is found in the 36°N, western North Pacific spectrum. At 36°N in the eastern North Pacific, the peak spectral energy density is at the longest scale and period with no dominant sense of propagation; however, variability of slightly higher frequency propagates westward. Energy in the right quadrant in both spectra at 40°N appears to be predominantly leakage from the left quadrant.

The biggest difference between these four spectra is the extent to which higher frequency and wavenumber variability occurs. The Kuroshio Extension spectrum at 36°N in the western North Pacific shows energy over a broad range of frequencies, with a maximum well away from the longest scales. The trough at the 12-month period is probably a remnant of the removal of bimonthly means. The Oyashio Extension spectrum at 40°N in the western North Pacific is somewhat redder than the Kuroshio Extension spectrum but retains a large amount of spectral energy density at higher frequencies and wavenumbers. In contrast, both eastern North Pacific spectra are far redder. (Recall that the spectra are normalized so that each has the same total amount of energy.)

A general feature of all four spectra is a tenfold decrease from peak energy at a wavelength of about 3°. The wavenumber falloff simply means that the true resolution of the XBT data is coarser than ½°, as discussed before for the k spectrum. A similar falloff in frequency common to all four spectra is not observed because there must always be a minimum amount of data in the two-month bin in order for gridded values to be produced.

Aliasing of incompletely resolved waves must affect these spectra, but because sampling is random, the aliased wave may produce a strip or curve of energy between the actual (ω, k) and the origin, as discussed in the Appendix. The observed curve of energy in the ω/k spectra could be produced by a peak at an incompletely resolved reduced wavelength which is smeared towards the origin. However, if there were such an isolated peak, studies discussed in the Appendix indicate that it would be partially passed by the XBT sampling and would yield a (reduced) peak at the proper (ω, k).

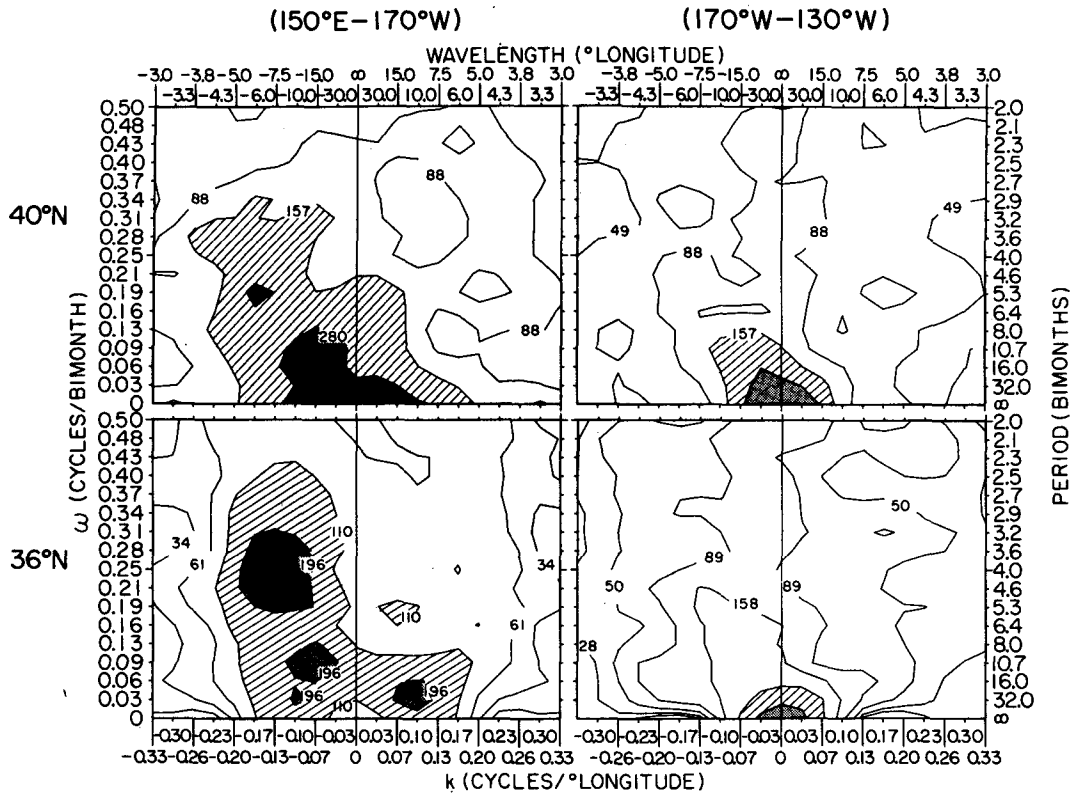

FIG. 10. Frequency–zonal wavenumber (ω/k) spectra of anomalous 300 m temperature for (a) the western and (b) eastern midlatitude North Pacific. Zonal wavelength is shown only to 2° although the Nyquist wavelength is 1°. (The effective Nyquist wavelength is between 3° and 4°.) Contour intervals are the 90% confidence intervals starting with a value slightly below the spectral maximum. The area within the first two contour levels below the maximum is shaded and the area within the third contour level is hatched.

The observations presented here confirm and extend results of previous analyses of this and similar datasets. Westward propagation has been a robust result of all previous analyses of such datasets in the North Pacific, beginning with Bernstein and White (1974). A tendency for eastward propagation in the Kuroshio Extension noted by Mizuno and White (1983) is also confirmed. The most important conclusion from these four spectra is that length and time scales in the Kuroshio Extension are shorter than elsewhere in the midlatitude North Pacific. The spectrum is reddest in the eastern Pacific; White and Tabata's (1986) ω/k spectrum along line *P* at approximately 50°N strongly resembles our 40°N spectrum for the eastern North Pacific.

d. Zonal-meridional wavenumber (k/l) spectra

The first half of the TRANSPAC XBT dataset has been used in previous two-dimensional wavenumber analyses. In the eastern and midlatitude North Pacific, Kang and Magaard (1980) found that the annual wavenumber vector which best fit a first baroclinic Rossby wave mode had a 400 km wavelength and propagated northwestward. Using standard two-dimensional spectral analysis, White (1985) found that the wavelength of the dominant interannual wavevector (with the annual signal removed) was about 1000 km with a period of 2 to 3 years, propagating both northwestward and southwestward. Both statistical treatments used the mesoscale filter described in section 3, although they used slightly different versions of the S2-gridded data. Caveats regarding resolution and aliasing which are indicated throughout the present paper apply as well to previous treatments of the TRANSPAC data.

A second group of statistical efforts to determine wavelength and propagation direction of interannual baroclinic Rossby waves in the eastern North Pacific use a time series along a single transect from Honolulu to San Francisco (Emery and Magaard, 1976; Price and Magaard, 1983). The vector component perpendicular to the transect was computed by assuming the Rossby wave dispersion relation. The bulk of vectors found indicated northwestward propagation, but were nearly orthogonal to the transect, suggesting that the wavevector was somewhat indeterminate. Wavelengths chosen a priori were on the order of 1000 to 1500 km and periods were from 12 to 28 months.

It appears that these earlier efforts to detect meridional propagation direction from k/l spectra using the TRANSPAC data are suspect, based on the present study. Two-dimensional wavenumber spectra for the western (150°E–170°W) and eastern (170°–140°W) North Pacific from 34° to 42°N were computed from the ½° gridded data and are shown in Fig. 11. There were 81 points in the zonal direction and 17 in the meridional direction; all observations were normalized by the standard deviation about the time mean at that grid point. Each zonal series and each meridional series was detrended and then each (x, y) matrix was detrended using a plane fit. A Tukey window with 40 lags in the zonal and 10 lags in the meridional direction was used. There were 7 and 6 bimonths (of a possible 48) for the western and eastern regions, respectively, with enough coverage to compute a spectrum for the ensemble average. Individual western and eastern midlatitude North Pacific spectra have 4 degrees of freedom so there are 28 and 24 degrees of freedom for the ensemble-averaged spectra in the western and eastern Pacific.

The k/l spectra for the eastern and western North Pacific differ although both have most energy at fairly long wavelengths in k and l, with a falloff at shorter wavelengths resulting from coarse resolution, S2 smoothing, and the actual spectral falloff. Both spectra are redder in l than k. A single peak occurs in the western North Pacific spectrum while three peaks occur in the eastern North Pacific spectrum. The single peak in the western North Pacific spectrum lies at longest meridional wavelengths and at somewhat shorter zonal wavelengths. The latter reflects the broad spectral peak in the zonal wavenumber spectra in the Kuroshio Extension (Fig. 8). Taken at face value, the western North Pacific k/l spectrum indicates predominantly zonal propagation with a slight southwestward tendency. (Because the k/l spectra are symmetric in the zonal direction, the direction of propagation to the east or west must be inferred from the ω/k spectra which indicate predominantly westward propagation in both regions.) The sampled region lies in and north of the Kuroshio Extension so it appears that, on average, propagation north of the Kuroshio Extension is southwestward. This is attractive because it suggests that the Kuroshio is a source of Rossby wave energy for the regions to the north and south, if southward phase velocity is associated with northward group velocity as it is in free Rossby waves. However, our experience with these spectra indicate that such an interpretation of propagation direction is not robust and depends on the form of the response function, as discussed later.

In the eastern North Pacific, one peak occurs at longest wavelengths and the other two at shorter wavelengths in k and l. The latter have southwestward and northwestward propagation based on the westward propagation found in the ω/k spectra. All peaks were evident in the k spectra, although the peaks at shorter wavelength were not especially pronounced.

The meridional shape of the k/l spectrum is suspect because of marginal data resolution; aliasing tests described in the Appendix showed that input plane waves shorter than 3.3° produce a correct spectral peak but part of the energy is aliased to longer wavelengths. The

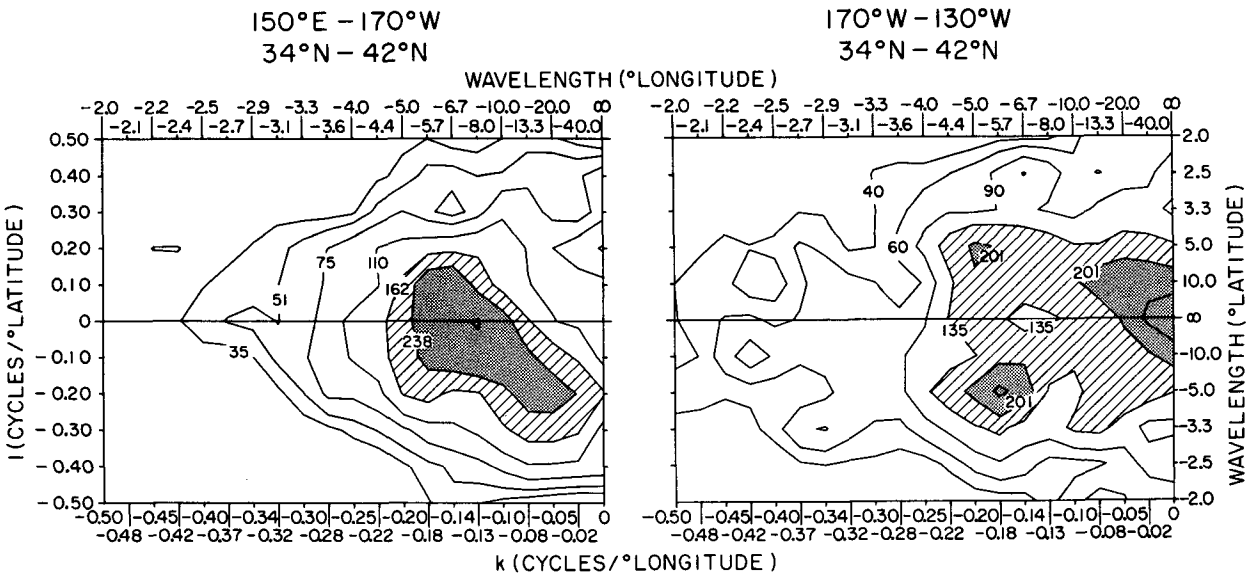

FIG. 11. Zonal–meridional wavenumber (k/l) spectra for (a) the western North Pacific (150°E–170°W, 34°–42°N) and (b) the eastern North Pacific (170°–130°W, 34°–42°N). Spectra were computed using 2° resolution in longitude and ½° resolution in latitude. Since actual resolution for the average data density is only slightly less than 2° in latitude and longitude, there is a steep falloff in spectral energy for wavelengths shorter than 4°. The spectra are shown only to 2° although the Nyquist wavelength is 1°. Contouring and shading are as in Fig. 10.

nature of the aliasing is more of a smearing than clean production of artificial peaks, so we feel fairly confident that any peaks we have found in the k/l spectra are not produced by aliasing. A bigger problem with correctly locating peaks and dominant propagation direction is noise: in contrast with the ω/k spectra where the spectral outlines were fairly well determined irrespective of the shape of the response function, the k/l spectra are far more dependent on the response function. Slight changes in the response function can alter the propagation direction from southwestward to due westward or even northwestward. Since there are relatively few realizations in the ensemble-averaged response function (and spectra), it is noisy and somewhat asymmetric (Fig. 14a). The slight asymmetry may be responsible for the southwestward tendency found in the k/l spectra, although the location of peaks is probably robust. The rolloff of the computed spectra is determined of course by both the actual rolloff, the data resolution, and S2 smoothing, as before, so the steepness of the spectrum cannot be estimated.

In summary, the k/l spectra of the western and eastern North Pacific differ. Propagation in the western North Pacific straddling and north of the Kuroshio Extension is zonal and may be slightly to the south, while propagation in the eastern North Pacific appears to be both northwestward and southwestward, based on additional information from the ω/k spectra.

6. Summary

The main thrust of this study was to present in a unified fashion the results of spectral analysis of the 8-year TRANSPAC XBT dataset which covers the midlatitude North Pacific. The original goal was to examine this dataset for the time and length scales of mesoscale variability in the midlatitude North Pacific and to determine the source of variability. The length of the dataset and sheer number of observations made such a study initially attractive. However, the TRANSPAC program was not designed to resolve the mesoscale in space or time; we have found that there are limitations to using it as a whole for mesoscale studies. Individual, well-sampled, synoptic lines within the dataset have proved useful for one-dimensional wavenumber spectra (Bernstein and White, 1977). There are limited areas in midlatitudes where there has been enough continuous, dense sampling to produce reasonable frequency spectra. However, there is not enough coverage to produce completely unaliased, one-dimensional k and ω spectra everywhere or two-dimensional ω/k and k/l spectra anywhere.

In order to sample as large an area as possible, we compromised in time and space coverage by choosing two-month time bins and restricting analysis to regions with resultant average observation separation of less than 1.65° latitude/longitude. Thus the Nyquist period and maximum Nyquist wavelength were four months and 3.3°. Because of uneven data density, local Nyquist wavelengths are shorter in many areas but a portion of energy at wavelengths of 1° to 3.3° is passed. Based on the typical bimonthly data distribution, average coverage is on the order of 1.25°. Aliasing tests showed that partially resolved waves (1° to 3.3° wavelength) produce peaks at the correct wavenumber with energy generally smeared into a strip at longer wavelengths; if additional peaks are produced, they have much lower energy than the peak at the correct input wavenumber.

To achieve acceptably less-aliased sampling in space and time, data density would have to be increased to the point where average station spacing is less than 1° within a period of 30 days, based on previous results which show high energy to wavelengths of 200 to 250 km and periods of 60 to 80 days. This means an eightfold increase in current sampling density, since 2° spacing is now achieved in each 60-day period over most of the midlatitude North Pacific. The sampling rate during the intensive observation period in 1980 tripled the usual rate and achieved better than 1° spacing in a 60-day period, with much higher sampling in the Kuroshio Extension. For temperature mapping, Koblinsky et al. (1984) recommend sampling rates of better than five samples per 300 km during each 15-day period; this is comparable to the requirement for relatively unaliased spectra.

Ignoring the aliasing problems, but not interpreting wavelengths shorter than 3° to 4°, we found:

1) a broader spectrum of variability in the Kuroshio Extension than elsewhere, including shorter length and time scales;
2) reddest wavenumber and frequency spectra in the eastern North Pacific with the time series dominated by an overall cooling trend and nearly zonally uniform patterns;
3) westward propagation throughout the region with additional eastward propagation only in the Kuroshio Extension;
4) northwestward and southwestward propagation in the eastern North Pacific, and zonal propagation with a tendency towards southwestward propagation in the western Pacific, based on meridional series which are quite short because of the gyre geometry.

The temperature and temperature anomaly fields showed the following features:

1) The standard deviation about the time mean is largest in the Kuroshio Extension and is low and nearly constant in the eastern Pacific;
2) anomalies of annual and semiannual cycle (bimonthly means with the overall time mean removed) are maximum at 38°N, two degrees north of the maximum of anomalies of other periods;
3) anomalies of annual and semiannual periods propagate away from the Kuroshio Extension in the western Pacific and propagate predominantly north-

westward in the eastern Pacific, based on maps of the anomalies themselves;

4) meanders in the mean temperature field in the western Pacific have larger gradients where baroclinic shear is northward (where $\partial T/\partial x$ is positive) than where shear is southward;

5) a cooling trend in the eastern Pacific occurred over the eight years of the dataset and was stronger at 40° than at 36°N.

Acknowledgments. We thank A. E. Walker for his programming, aid in data analysis, and general input. This work was supported by the Office of Naval Research through Contracts N00014-80-C0440 and N00014-85-C0104 to Scripps Institution of Oceanography.

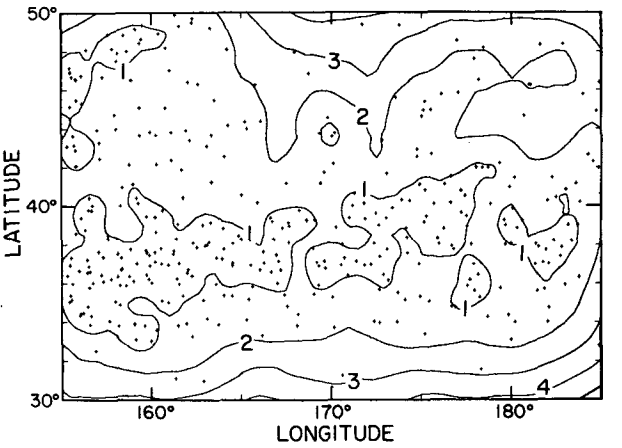

FIG. 12. XBT locations and $\bar{r}_8$ for February–March 1982 (as in Fig. 2), used for the spectral tests conducted on plane waves shown in Fig. 13.

APPENDIX

Sampling Tests

Because sampling in the TRANSPAC dataset is irregular, the only way to determine the response function for the method and the extent of spatial aliasing is to test known inputs. Plane waves and random numbers are used to test aliasing and to construct response functions for each type of spectrum. We find that there is an effective Nyquist wavelength based on the average separation between neighboring points; this may seem to contradict a sampling theorem which indicates that there is no aliasing if sampling is random. However, this theorem applies to infinite data series with an infinite number of chances to sample each wavelength. Clearly this is not the case for a dataset which is confined to an ocean basin.

1. Aliasing

Two-dimensional plane waves, $\cos(kx + ly)$, were assigned to XBT observation positions. Sixteen individual waves were analyzed. All input waves were in the second quadrant ($k < 0$, $l > 0$); wavelengths in x and y were 3.1°, 4.4°, 7.3° and 22°. Four tests were performed for each wave. The first test was a control with each wave assigned to a regular ½° grid. In the second test, the wave was assigned to XBT locations for February/March 1982, and then gridded at ½° intervals using S2. In the third test, the wave was assigned to ½° intervals and spectral analysis was restricted to regions where $\bar{r}_8$ was less than 2°. The fourth test was the same as the second but with gridding to 2° intervals. The February/March 1982 bimonth was selected because it had average-to-good data coverage; Fig. 12 shows the locations of all observations used.

Three measures of performance of the four spectra were used. The first was the amount of energy at the input wavenumber relative to the total energy in the spectrum; for unaliased waves, this is a measure of bias. The second measure was the relative amount of energy at wavelengths longer than the input wave; for unaliased waves, this is also a measure of bias, while for aliased waves, the increase in this fraction above its value for unaliased waves is an indication of the amount of aliasing. The third measure was the relative amount of energy found in the quadrant of the input wavenumber; again this indicates the effect of aliasing for less well-resolved waves since aliasing can occur from one quadrant to another. Figure 13 shows these performance measures for a subset of the sixteen waves and is described in the next few paragraphs.

In the control set of spectra of plane waves assigned to a regular ½° grid, a peak is placed correctly at the input wavenumber with 20% of the total energy (Fig. 13a); this is independent of wavenumber because no waves are aliased. The spread about the peak is due to bias. The fraction of energy spread to longer wavelengths lower than the input wave is independent of wavenumber and is about 32% (Fig. 13b). The fraction of energy in the input quadrant is quite high (>90%) and is also nearly independent of input wavenumber (Fig. 13c).

When plane waves are sampled at all XBT locations shown in Fig. 12 and then interpolated to a ½° grid using S2, the results are quite different from regular ½° sampling. The average separation of nearest points varies from 0.8° to greater than 3.3° ($\bar{r}_8$ from 1° to more than 4° at the perimeter). Aliasing of the shortest tested waves (3.1° and 4.4°) is expected since they are resolved only in some portions of the sampled region. Nevertheless, the dominant peak in each of the 16 spectra is at the input wavenumber, indicating that all tested waves are resolved fairly well somewhere in the region. However, there is a dramatic reduction in energy at the peak from the longest waves, which are well resolved by the XBTs, to waves with one component shorter than 6°, which are not as well resolved. In addition, spectra of waves with at least one component

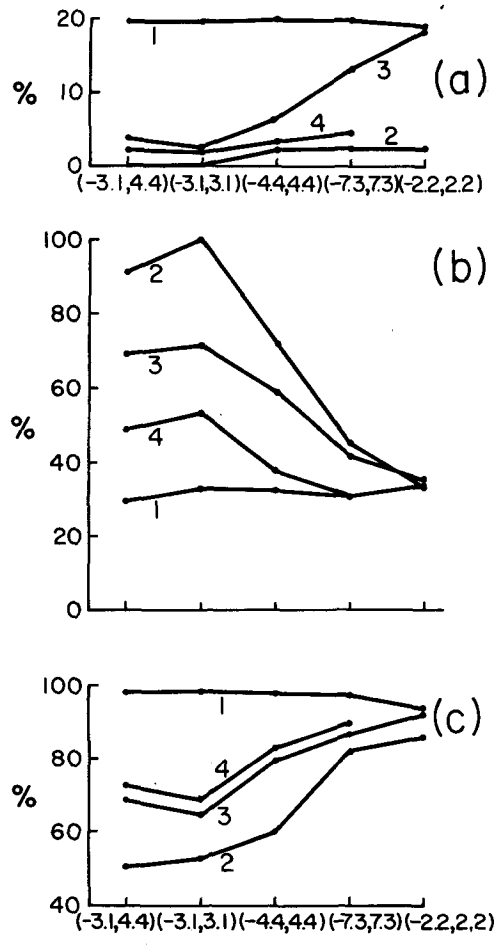

FIG. 13. (a) Percent of energy at the input wavevector relative to the total energy. (b) Percent of energy at wavelengths in both quadrants longer than the input wavelength relative to the total energy. (c) Percent of energy in the second quadrant (the quadrant of the input plane waves) relative to the total energy. Sixteen waves with wavelengths 3.1°, 4.4°, 7.3°, and 22° in each direction were used in the test; only values from the diagonal wavevectors (−3.1°, 3.1°), (−4.4°, 4.4°), (−7.3°, 7.3°), and (−22°, 22°) and one off-diagonal wavevector (−3.1°, 4.4°) are shown. The curve labels are 1) regular ½° sampling; 2) values gridded by S2 to a 2° grid; 3) values gridded by S2 to a ½° grid; 4) values gridded by S2 to a ½° grid and subject to the constraint that $\bar{r}_8 < 2°$.

at 3.1° or 4.4° have a second and sometimes third peak at much longer wavelengths (∞, 22°, or 11°); the quadrant in which these "aliases" occur is unpredictable. Aliasing occurs predominantly to longer waves; this is not the case for waves which are sampled regularly and which are aliased in a Brillouin pattern. The fraction of energy found at wavelengths longer than the input wave (Fig. 13b) varies from 32% at the longest wave to 72% at the shortest wave (−3.1°, 3.1°). Thus there is as much as 40% more energy at longer wavelengths when the waves are poorly resolved, despite the presence of a dominant peak at the input wavevector. A high percentage of energy remains in the input quadrant at the longest, best-resolved waves (more than 90%) while the worst-resolved waves lose energy to the opposite quadrant (Fig. 13c).

Reasonable improvement is achieved when only regions where $\bar{r}_8$ is less than 2° are used. When the 16 plane waves are sampled at XBT locations in the region 33°–42°N and 155°E–175°W and gridded at ½° intervals (Fig. 12), all measures of aliasing show improvement. For each wave, there is a peak at the correct input wavenumber; unfortunately, the relative amount of energy in the peak is greatly reduced compared with the previous test in which all XBT locations were used because the size of the region is reduced. Some aliasing of energy to longer waves from the shorter ones occurs, but only the shortest waves create additional peaks. Six of the 16 waves produce additional peaks, three of which are at the correct aliased wavenumbers associated with regular sampling with a 3° to 4° Nyquist wavelength, corresponding to the worst-resolved areas. (In contrast, 8 of the 16 waves produced one additional peak in the preceding test and 3 produced two additional peaks.) There is significant improvement in the amount of energy aliased to lower wavenumber: the amount of energy in both quadrants at longer wavelengths than the input wave ranges from 53% at the shortest waves (instead of 72%) to 32% at the longest, the fraction found for completely unaliased waves (Fig. 13b). The amount of energy in the quadrant of the input waves varies from 68% to 89% of the total energy from the shortest to the longest waves (Fig. 13c), a small improvement over the preceding test where the range was 64% to 92%.

Based on these tests, it appears that spectral results are improved if only those regions where $\bar{r}_8$ is less than 2° are used. Greater improvement would be achieved by choosing a smaller $\bar{r}_8$ (less than 1° would be ideal based on previous studies of length scales in the North Pacific) but coverage would be extremely restricted. Since we will use the criterion that $\bar{r}_8$ be less than 2° in selecting regions for subsequent analysis, the effective Nyquist wavelength is less than about 3.3°. This leads us to ask whether it would be wiser to use a 2° rather than a ½° grid, given that resolution is only 2° on the region's periphery. The answer is no, because the amount of aliasing increases greatly when a 2° grid is used, since shorter waves really can be resolved in some areas by the XBTs. To check that 2° spacing actually causes more aliasing than ½° spacing, the tests were run on input waves sampled at XBT locations and gridded at 2° intervals. All waves but the very longest produced two or three additional peaks, energy at the input wavenumber peak was low (Fig. 13a), and a large amount of energy from the shortest waves was found in the wrong quadrant as a result of aliasing (Fig. 13c). It is thus best to err on the side of oversampling when selecting a grid. It is extremely important to remember that the Nyquist wavelength depends on the actual XBT sampling density and not on the arbitrary choice of grid spacing.

Quantifying the amount of aliasing is difficult because it depends on wavenumber, direction, and sampling; it can be done only empirically. Based on these tests, there is a weak Nyquist wavelength at about 3.3°, but because data density varies, the Nyquist region will be fuzzy and broad and will depend on the precise sampling. Roughly 20% of the energy at wavelengths shorter than 4° is aliased to long waves and roughly 20% of the energy at wavelengths shorter than 4° will be found in the wrong quadrant, creating some ambiguity in determining propagation directions.

2. Response function

The response function for the S2 gridding procedure and spectral method was computed empirically. The S2 method is essentially a smoothing procedure, a low-pass filter with variable averaging radius which depends on data density. All procedures used in treating observed data were performed on normally distributed random numbers which were assigned to all XBT locations in the area 30°–50°N, 150°E–130°W from June 1976 to April 1984. Procedures followed were to grid the random numbers using S2, select regions where $\bar{r}_8$ was less than 2°, and then to compute the k, ω, ω/k and k/l spectra of the gridded random numbers. The spectral procedures were described in section 5. Any aliasing problems in spectra of the actual data are enhanced in those of the random data since the former are inherently red and the latter white. Since the actual spectra discussed in section 5 are recolored by division by the empirically determined response function, the spectra shown in Figs. 8 to 11 are somewhat whiter than the true spectra. However, we felt that the most important issue was to eliminate as many artificial effects of the data processing and spectral procedures as possible; this was best accomplished by dividing the spectra by the response function.

Response functions are shown in Fig. 14. One-dimensional zonal wavenumber (k) and frequency (ω) spectra and two-dimensional (ω/k) and (k/l) spectra are shown for 40°N, 150°E–170°W. The k spectrum is an ensemble average of 277 individual spectra. It shows the obvious redness associated with the S2 smoothing and drop at lowest k due to detrending. Response functions for all k spectra shown in section 5 were nearly identical, indicating that coverage in each area was nearly the same. Degradation (increased redness) due to poorer resolution was evident only at 34°N and justifies restricting analysis to the region used.

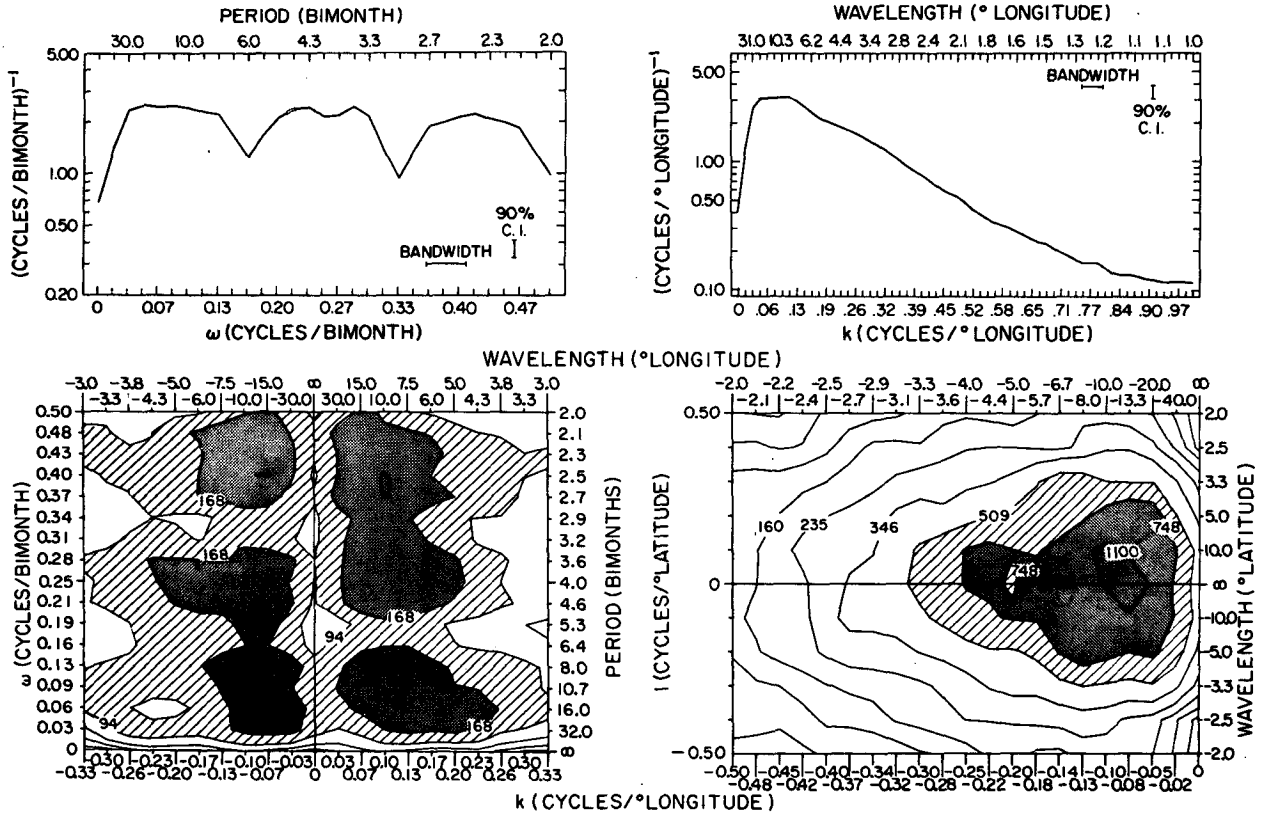

FIG. 14. Response functions: average spectra of normally distributed random numbers, assigned to actual XBT observations and gridded by S2. (a) Frequency, (b) zonal wavenumber, (c) frequency–zonal wavenumber, and (d) zonal–meridional wavenumber. Contouring and shading for the two-dimensional spectra are as in Fig. 10.

The ω spectrum is an average of 38 spectra, one every five degrees along 36° and 40°N. The ω response function is dominated by troughs at 12, 6 and 4 months, the least also being the Nyquist period. The drop at lowest frequency is due to detrending. Otherwise the response function is fairly white.

The ω/k response function is the average from the four different areas of the North Pacific. It clearly shows general redness in the k spectrum resulting from detrending and S2 smoothing, and troughs at 4, 6 and 12 months resulting from removal of bimonthly means.

The k/l response function is an average of 13 realizations. It is basically red in l and k and shows the effect of detrending at lowest k, resulting in a peak removed from the origin along the k axis. Detrending had virtually no effect in l; perhaps the peak is shifted a short distance from the axis but is undetected because the series is so short.

The two tests described in this Appendix show that 1) S2 effectively curtails power at wavelengths shorter than 3°, given the actual density of TRANSPAC observations for two-month periods, and 2) the best procedure of the choices that were examined is to grid the data at regular ½° intervals and select only regions where $\bar{r}_8$ is less than 2°. No spectral procedure can eliminate the aliasing of wavelengths shorter than 3° to 4°, associated with a two-month time bin. Improvement would result from greater restriction on areas used for spectral analysis and the use of a shorter time bin; however, this severely curtails the amount of data that can be used in the analysis.

REFERENCES

Bernstein, R. L., and W. B. White, 1974: Time and length scales of baroclinic eddies in the central North Pacific Ocean. *J. Phys. Oceanogr.*, **4**, 613–624.

——, and ——, 1977: Zonal variability in the distribution of eddy energy in the mid-latitude North Pacific Ocean. *J. Phys. Oceanogr.*, **7**, 123–126.

——, and ——, 1981: Stationary and traveling mesoscale perturbations in the Kuroshio Extension Current. *J. Phys. Oceanogr.*, **11**, 692–704.

——, and ——, 1982: Meridional eddy heat flux in the Kuroshio Extension Current. *J. Phys. Oceanogr.*, **12**, 154–159.

Emery, W. J., and L. Magaard, 1976: Baroclinic Rossby waves as inferred from temperature fluctuations in the eastern Pacific. *J. Mar. Res.*, **34**, 365–385.

Fu, L.-L., 1983: On the wavenumber spectrum of oceanic mesoscale variability observed by the SEASAT altimeter. *J. Geophys. Res.*, **88**, 4331–4341.

Harrison, D. E., W. J. Emery, J. P. Dugan and B.-C. Li, 1983: Mid-latitude mesoscale temperature variability in six multiship XBT surveys. *J. Phys. Oceanogr.*, **13**, 648–662.

Hasunuma, K., and K. Yoshida, 1978: Splitting of the Subtropical Gyre in the western North Pacific. *J. Oceanogr. Soc. Jpn.*, **34**, 160–172.

Kang, Y. Q., and L. Magaard, 1980: Annual baroclinic Rossby waves in the central North Pacific. *J. Phys. Oceanogr.*, **10**, 1159–1167.

Kawai, H., 1972: Hydrography of the Kuroshio Extension. *Kuroshio: Physical Aspects of the Japan Current*, Ed. H. Stommel, and K. Yoshida, U. Washington Press, 235–352.

Kitano, K., 1975: Some properties of warm eddies generated in the confluence zone of the Kuroshio and Oyashio Currents. *J. Phys. Oceanogr.*, **5**, 245–252.

Koblinsky, C. J., R. L. Bernstein, W. J., Schmitz and P. P. Niiler, 1984: Estimates of the geostrophic stream function in the western North Pacific from XBT surveys. *J. Geophys. Res.*, **89**, 10 451–10 460.

Levine, E. R., and W. B. White, 1983: Bathymetric influences upon the character of North Pacific fronts, 1976–1980. *J. Geophys. Res.*, **88**, 9617–9625.

Mizuno, K., and W. B. White, 1983: Annual and interannual variability in the Kuroshio Current system. *J. Phys. Oceanogr.*, **13**, 1847–1867.

Mysak, L. A., 1983: Generation of annual Rossby waves in the North Pacific. *J. Phys. Oceanogr.*, **13**, 1908–1923.

Pierson, W. L., Ed., 1960: The directional spectrum of a wind generated sea as determined from data obtained by the stereo wave observation project. *Meteor. Papers*, **2**(6), 88 pp.

Price, J. M., and L. Magaard, 1980: Rossby wave analysis of the baroclinic potential energy in the upper 500 meters of the North Pacific. *J. Mar. Res.*, **38**, 249–264.

——, and ——, 1983: Rossby wave analysis of subsurface temperature fluctuations along the Honolulu–San Francisco great circle. *J. Phys. Oceanogr.*, **13**, 258–268.

Roden, G., 1970: Aspects of the mid-Pacific transition zone. *J. Geophys. Res.*, **75**, 1097–1109.

——, 1972: Temperature and salinity fronts at the boundaries of the subarctic and subtropical transition zones in the western Pacific. *J. Geophys. Res.*, **77**, 7175–7187.

Sampson, R., 1973: Users manual for SURFACE II graphics system. Kansas Geological Survey, University of Kansas, 144 pp.

White, W. B., 1977. Annual forcing of baroclinic long waves in the tropical North Pacific Ocean. *J. Phys. Oceanogr.*, **7**, 50–61.

——, 1982: Traveling wave-like mesoscale perturbations in the North Pacific Current. *J. Phys. Oceanogr.*, **12**, 231–243.

——, 1985: The resonant response of interannual baroclinic Rossby waves to wind forcing in the eastern midlatitude North Pacific. *J. Phys. Oceanogr.*, **15**, 403–415.

——, and R. L. Bernstein, 1979: Design of an oceanographic network in the midlatitude North Pacific. *J. Phys. Oceanogr.*, **9**, 592–606.

——, and ——, 1981: Large-scale vertical eddy diffusion in the main pycnocline of the central North Pacific. *J. Phys. Oceanogr.*, **11**, 434–441.

——, and Y.-H. He, 1986: Interannual variability in the heat content of the Kuroshio Extension associated with the 1982 ENSO event. *J. Phys. Oceanogr.*, **16**, 309–321.

——, and J. F. T. Saur, 1981: A source of annual baroclinic waves in the eastern subtropical North Pacific. *J. Phys. Oceanogr.*, **11**, 1452–1462.

——, and ——, 1983: Sources of interannual baroclinic waves in the eastern subtropical North Pacific. *J. Phys. Oceanogr.*, **13**, 531–544.

——, and S. Tabata, 1987: Interannual westward propagating baroclinic long-wave activity on line *P* in the eastern midlatitude North Pacific. *J. Phys. Oceanogr.*, **17**, 385–396.

——, R. L. Bernstein, G. McNally, S. Pazan and R. Dickson, 1980: The thermocline response to transient atmospheric forcing in the interior midlatitude North Pacific 1976–1978. *J. Phys. Oceanogr.*, **10**, 372–384.

Wilson, W. S., and J. P. Dugan, 1978: Mesoscale thermal variability in the vicinity of the Kuroshio Extension. *J. Phys. Oceanogr.*, **8**, 537–540.